TU/e EINDHOVEN UNIVERSITY OF TECHNOLOGY

Eindhoven University of Technology

MASTER

Three-dimensional magnetostatic field of a video head

Savelkoul, J.F.G.M.

Award date:
1983

Link to publication

21 FEB. 1984

Prof. Dr. M.P.H. Weenink / T.H. Eindhoven

26-2-'84

NAT.LAB. REPORT 5895

J.F.G.M. Savelkoul* and
S.B. Luitjens

THREE-DIMENSIONAL MAGNETOSTATIC
FIELD OF A VIDEO HEAD

ET-19-83

8222 256 95021

PHILIPS

THREE DIMENSIONAL MAGNETOSTATIC FIELD
OF A VIDEO HEAD

Period of work: Dec. 1982 - Sept. 1983
Notebooks: none

* This study has been made in fulfilment of the requirements
  for the Degree of Master of Science (Ir.) at the Eindhoven
  University of Technology, Department of Electrical
  Engineering, under the supervision of
  Prof.Dr. M.P.H. Weenink, Eindhoven University of
  Technology and
  Dr.Ir. S.B. Luitjens, Philips Research Laboratories,
  Eindhoven.

8222 256 95021

SUMMARY

This report treats the three-dimensional calculation of the magnetic field strength of a video head, excited by a permanent magnet, which is a model for the head's coil. With the help of the magnetic field strength at the position of the tape, the side reading of the low frequency track following signal by the constriction of the head can be studied.

The calculations are done with the program package PADDY, that uses a finite element method for solving magnetostatic problems. With the PADDY results also the efficiency and the self inductance of the head are calculated.

The numerical Fourier Transform of these results is complicated by the relatively small number of "field points" in a finite part of 3D-space. Therefore an analytical model is proposed, that consists of magnetically charged plates. With this model the effect of the constriction can be described properly. The surface charge on these plates is chosen considering the results of PADDY. This model is a first step towards a proposed method, which allows calculation of the magnetic field in every point in space (in principal). This method uses the surface charge density of the head, that can be obtained from the PADDY results.

J. Savelkoul
Eindhoven,
11-10-'83

PHILIPS

THREE-DIMENSIONAL MAGNETOSTATIC FIELD OF A VIDEO HEAD

CONTENTS: PAGE

PHILIPS

CHAPTER ONE

GENERAL INTRODUCTION AND BACKGROUND OF THE PROBLEM

1.0. INTRODUCTION

1.1. WHY THREE DIMENSIONAL?

1.2. THE APPLICATION OF THE CONSTRICTION IN A VIDEO HEAD

1.3. THE EFFECT OF THE CONSTRICTION IN A VIDEO HEAD

1.4. SOME RESULTS OF MAGNETIC RECORDING THEORY

1.0. INTRODUCTION

In this chapter a brief introduction into magnetic re-
cording is given. The question why the calculation of the
magnetic field should be three dimensional, is treated. The
major problem in increasing track density: crosstalk, is
discussed and an application of it in the V2000 systems is
given. Finally some results of magnetic recording theory are
presented and their importance is elucidated.

1.1. WHY THREE DIMENSIONAL?

To answer this question we have to obtain some insight into the magnetic recording process.

The magnetic recording process transforms a time varying electrical signal, representing the information to be stored, into a pattern of spatially varying magnetization in a magnetizable medium (write process, Figure 1.1a). This is achieved by moving the magnetizable medium, with constant velocity, past a write head. The write head transforms the electrical signal into a time-varying magnetic field, which in its turn, magnetizes the medium: the information is stored.

When the stored information has to be reproduced, the medium is moved past the read head. The read head transforms the spatially varying pattern of magnetization into an electrical signal (read process, Figure 1.1b), which after being properly processed, can be made to resemble the original · write current (Van Herk, 1980).
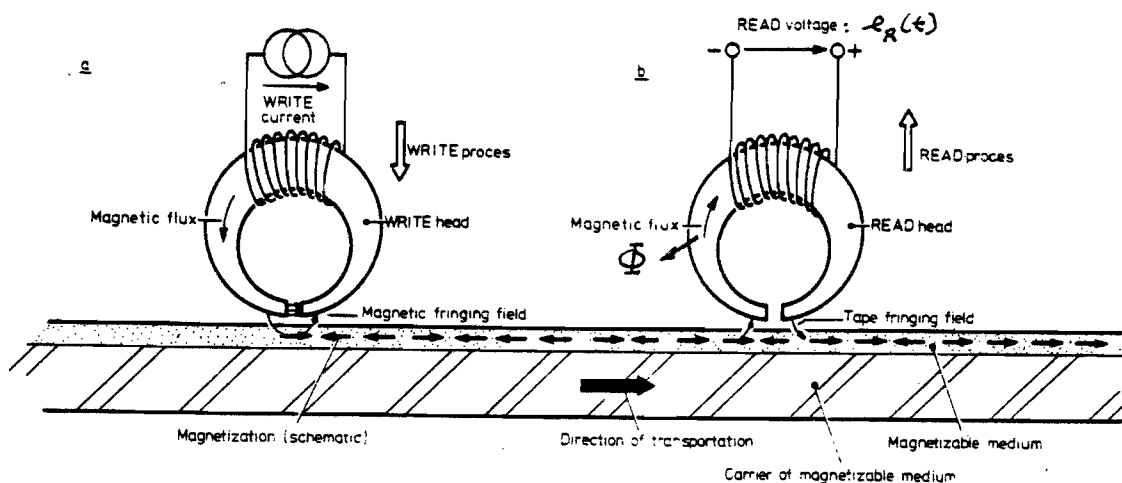
Figure 1.1

The magnetic medium is usually a tape or a disk, on which the information is stored in straight or circular tracks. These tracks are lying side by side in a thin magnetic layer on a non-magnetic carrier material. When the electrical signal is represented by the variation of the magne-

tization in the direction of transportation of the medium, we have the so-called longitudinal recording mode (Figure 1.2). The other directions of magnetization mentioned in Figure 1.2 are related to transverse and perpendicular recording.

Up to now most recording systems operated in the longitudinal mode. However since the paper of Iwasaki and Nakamura (1977) much effort has been put into developing systems that use the perpendicular mode. In this report we will concentrate on the longitudinal process.
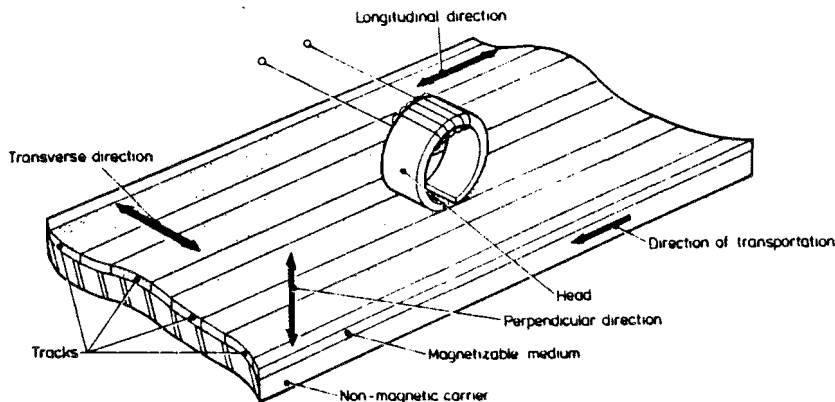
Figure 1.2

An account of the fact that magnetic recording techniques are of widespread use for storing a tremendously growing amount of information, there is a constant demand for higher storage capacity. One of the important parameters governing this storage capacity, is the width of the tracks that are recorded on the magnetic medium.

At the beginning of magnetic recording the first recorders that utilized a flat tape, needed the entire tape width for recording a single track in the longitudinal mode. To increase storage capacity the track width was reduced and more tracks were laid side by side on the tape. It was soon discovered that a drastic reduction of the track width and of the distance between adjacent tracks leads to difficulties.

The source of these difficulties is the fringing field of the head illustrated in Figure 1.3.
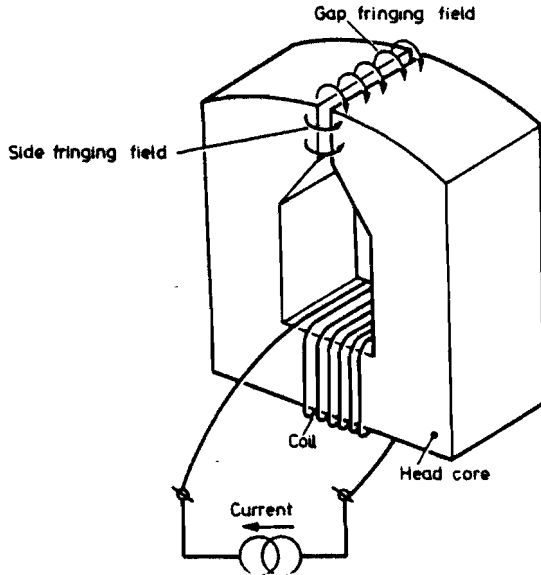
Figure 1.3

Its influence on the write and read properties of the head can be distinguished into several adverse effects (Van Herk 1980). Two of them are: the side writing and the cross-talk of adjacent tracks. They put a primary limitation on the track density available (Figure 1.4).
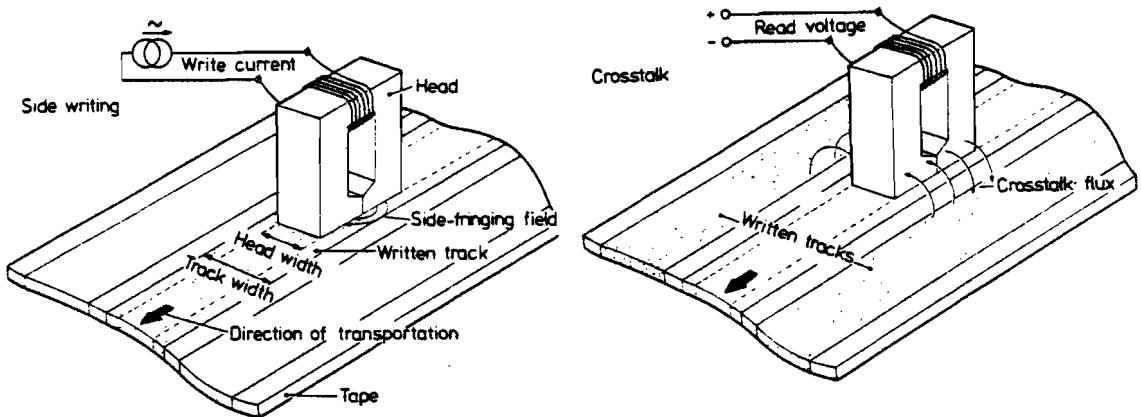
Figure 1.4

With the help of the reciprocity theorem in magnetic recording theory it can be made clear, that the structure of the magnetic field external to a magnetic recording head determines, through its introduction with the recording medium, the recording and reproduction properties of the configuration (De Hoop, 1977). In the fifties Westmijze (1953) and Karlqvist (1954) already published a theoretical analysis of this field. These calculations, however, were based on a two-dimensional approximation of the problem. This means that the resulting field has only an x and an y component which are independent of the z coordinate.

The field of the structure in Figure 1.5 is properly described in the symmetry plane z=0 by means of a two dimensional approach. For $L \gg d_1$ and $L \gg d_2$ this approximation is valid for $|z| < 1/2L$. Near $|z| = 1/2L$ the field is not properly described anymore.
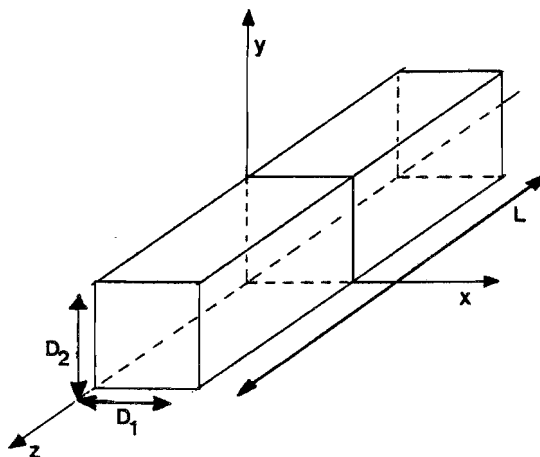
Figure 1.5

For a one track recording system a two dimensional description of the field is sufficient, since there are no neighbouring tracks in the z direction.

The relative dimensions of today's magnetic heads in smalltrack-recording systems make, that certain characteristic effects cannot be described with only an x and an y dependence of the field components. One of these effects is crosstalk. Since it is our goal to investigate this phenome-

non, the dependence of the field components of the z coordinate should be taken in account. So the calculation should be <u>three dimensional</u>.

The consequence is that the calculation cannot be done analytically for an arbitrary magnetic head. Only for special head analytical three-dimensional expressions for the field exist, for instance: "the infinite-wedge modes (Van Herk, 1977)". So for practical heads a numerical calculation is needed.

1.2. THE APPLICATION OF CROSSTALK IN THE V2000 SYSTEMS

In the previous paragraph we described crosstalk as a troublesome phenomenon, that restricts the density of tracks. Yet crosstalk can be made useful, as will be shown below.

Available consumer video-recorders record the tracks with the so-called "helical-scan" process. With this technique the tracks are written inclined on the tape. The video-2000 systems use a track width of 22 micrometer. To position the heads on the right track, Dynamic Track Following (D.T.F.) is used (Bahr 1981). In the explanation of D.T.F. and throughout the rest of this report we shall denote the track, the head should be positioned on with: "the actual track".

Figure 1.6 shows the read signal caused by a track of width 22 micrometer and read with a head of the same width. The recorded signal in Figure 1.6 has a wavelength of 50 μm. This is a low frequency signal, since the velocity with which head and tape move relative to each other is 5 m/sec (V2000).
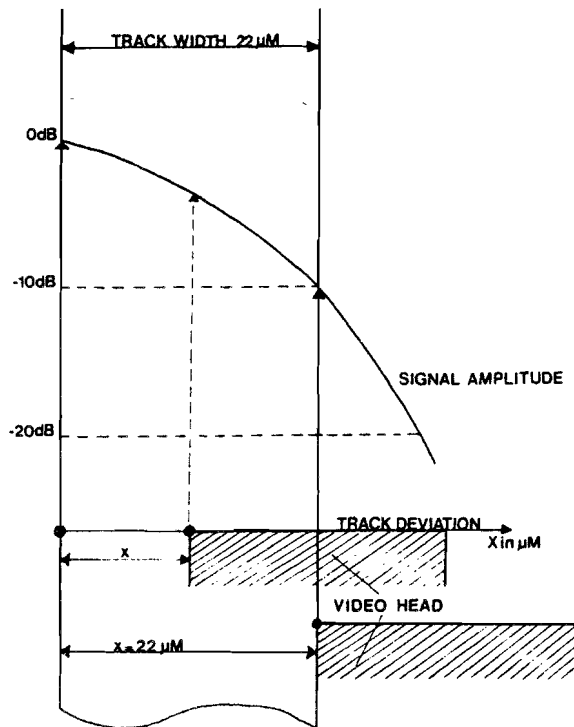
Figure 1.6

For such a signal it can be seen, that when the head is positioned exactly next to the actual track, the amplitude of the read signal decreases 10 dB. From this figure it is clear, that the signal loss is an indication for the position of the head relative to the actual track. If it would be possible to distinguish between the amplitudes of the low-frequency signals of the two neighbouring tracks, seen by the video head as crosstalk, one could develop a control loop: The head should be moved in the direction of the crosstalk signal with the lower amplitude until both measured amplitudes are equal. This is illustrated in Figure 1.7.
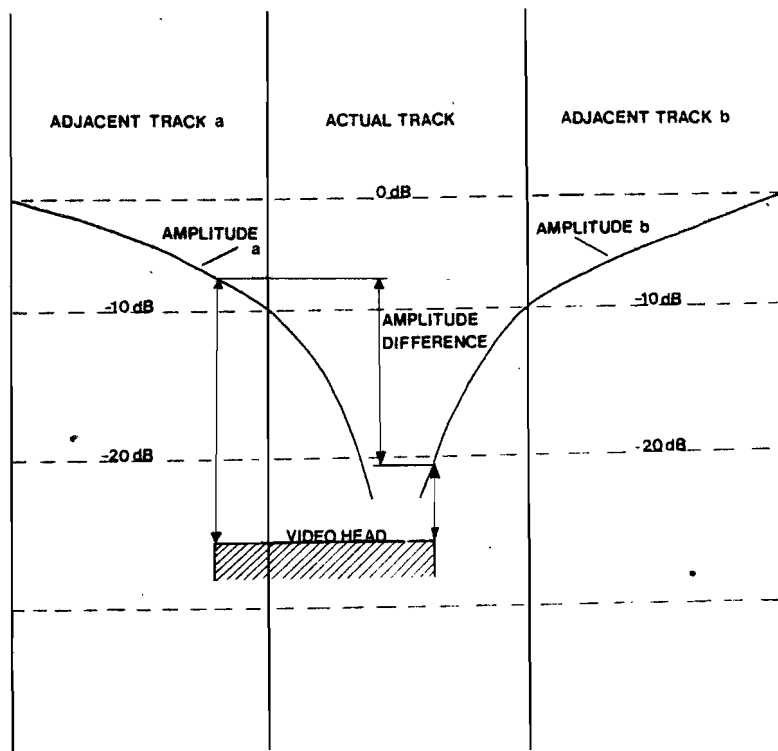
Figure 1.7

A way to distinguish between the crosstalk signals is to see to it, that they have different frequencies. In order to create these frequencies, during recording on each four successive tracks low frequency signals are written (Figure 1.8a). The order is given by Figure 1.8b.
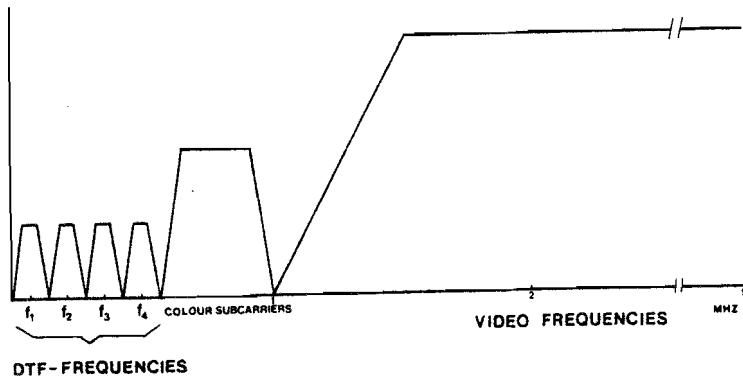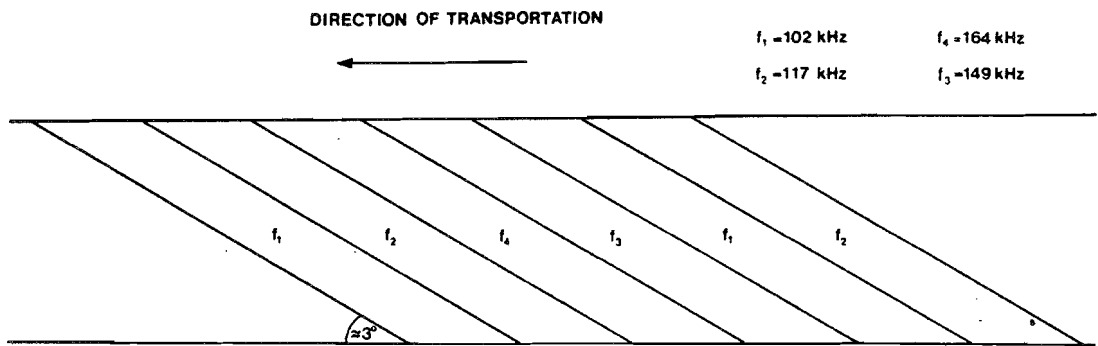
Figure 1.8a

Figure 1.8b

The frequencies $f_1, \ldots, f_4$ are chosen in such a way,
that mixing the low frequency signal of the actual track
with the low frequency crosstalk of the adjacent tracks,
always gives two signals of 15 kHz and 47 kHz. By comparing
the amplitudes of these signals a decision can be made in
which direction the head should be moved, in order to posi-
tion it exactly on the actual track. So the head should be
movable in the upward and downward direction (Figure 1.9).
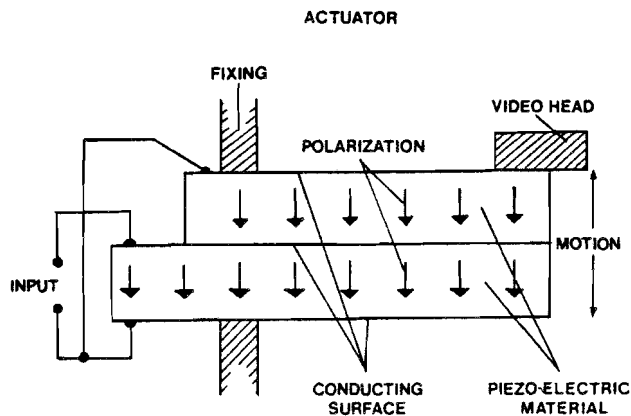
Figure 1.9

In order to make the head movable, it is placed on a so-called actuator (Figure 1.9). It consists of two polarized piezo-electrical plates, which are partly placed over each other, as shown in Figure 1.10. Dependent on the polarity of the applied control voltage the head can be moved upwards and downwards.

UPPER PART OF DRUM

PIEZO-ELECTRIC MATERIAL

video head

MAGNETIC TAPE

LOWER PART OF DRUM
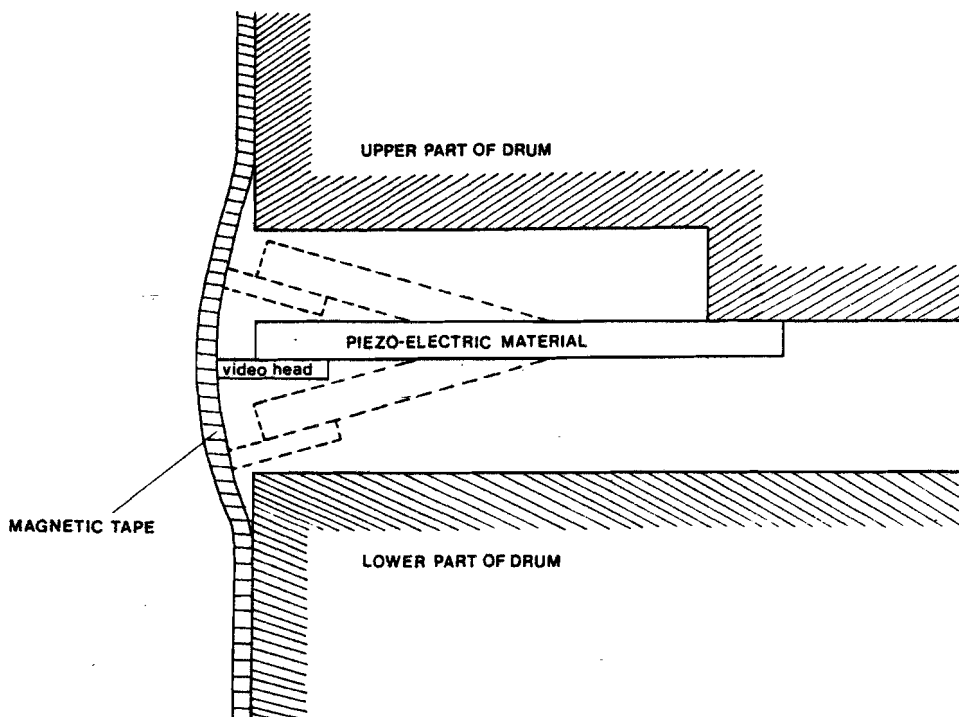
Figure 1.10

So the crosstalk phenomenon has been used to solve the problem of the positioning of the head. The consequence for the shape of the head to achieve optimum tracking will be discussed in the next section.

1.3. THE EFFECT OF THE CONSTRICTION IN A VIDEO HEAD

For the track following system as described in the former section a head is needed, which reads the low frequency information and suppresses the high frequency components. A magnetic head that displays such a function in the ring head with constriction, that is applied in the V2000 systems. To understand the operation of such a head, we shall elucidate the ring head itself first.

The head consists of an annular core of magnetic material. This "ring" is interrupted by an air gap (Figure 1.11), where a fringing field is present during the write process. This field exceeds the coercive force of the medium over slightly more than the entire width of the head: the information is recorded on a track.

Plane of symmetry
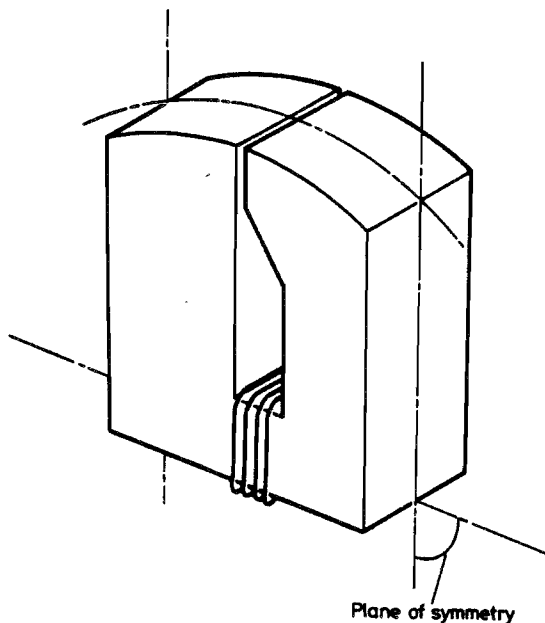
Figure 1.11

In the read process the magnetic medium moves relatively to the head and causes a change in the magnetic flux Φ (Wb) that is coupled into the head at the gap. The induced read voltage $\ell_R(t)$ at the terminals of the coil (n turns) is given by Faraday's law:

$$e_R(t) = -n\,\frac{d\Phi}{dt} \qquad\qquad 1.1$$

When a sinusoidal magnetization pattern is present on the medium, we can observe an interesting feature in the read voltage. At a wavelength near the gap length (G) $e_R(t)$ is zero. This phenomenon is called the gaploss effect. The reason for its occurrence is that at this wavelength, no flux is coupled into the head. The same behaviour can be noticed at G/ = 1,2,3,.... So we can define a gaploss function (Westwijze, 1953):

$$\frac{\sin(\pi G/\lambda)}{(\pi G/\lambda)} \qquad\qquad 1.2$$

Therefore ring heads are used for frequencies lower than the frequency corresponding to the gap length.

In order to suppress the high frequency signals of the adjacent tracks, these tracks should be read with a head with a relatively large gap. Meanwhile the actual track should be read with a very small gap. To satisfy these seemingly contradictory demands, a constriction is made in the ring head. Figure 1.12a shows the pole-face after the constriction is made.
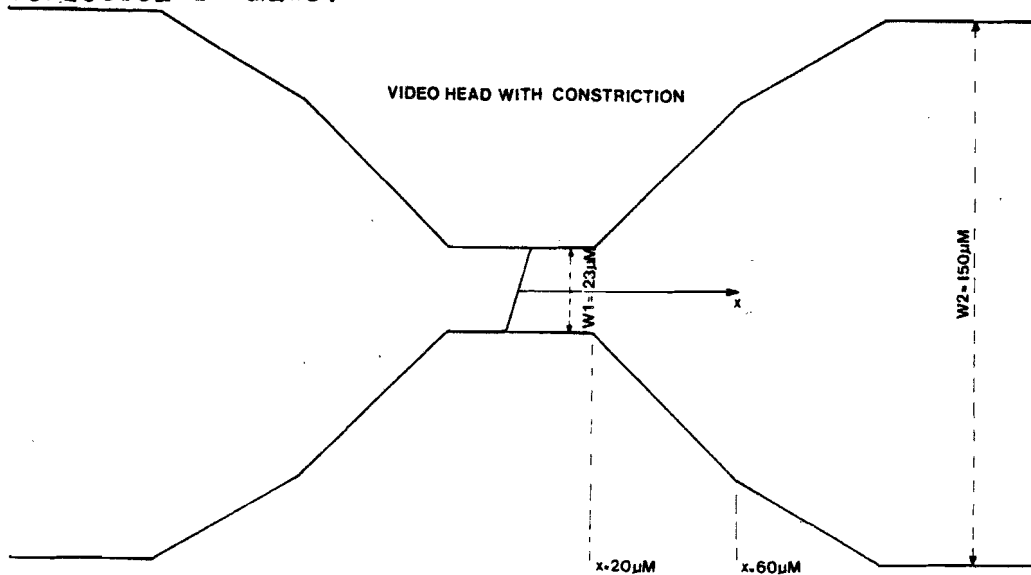
VIDEO HEAD WITH CONSTRICTION
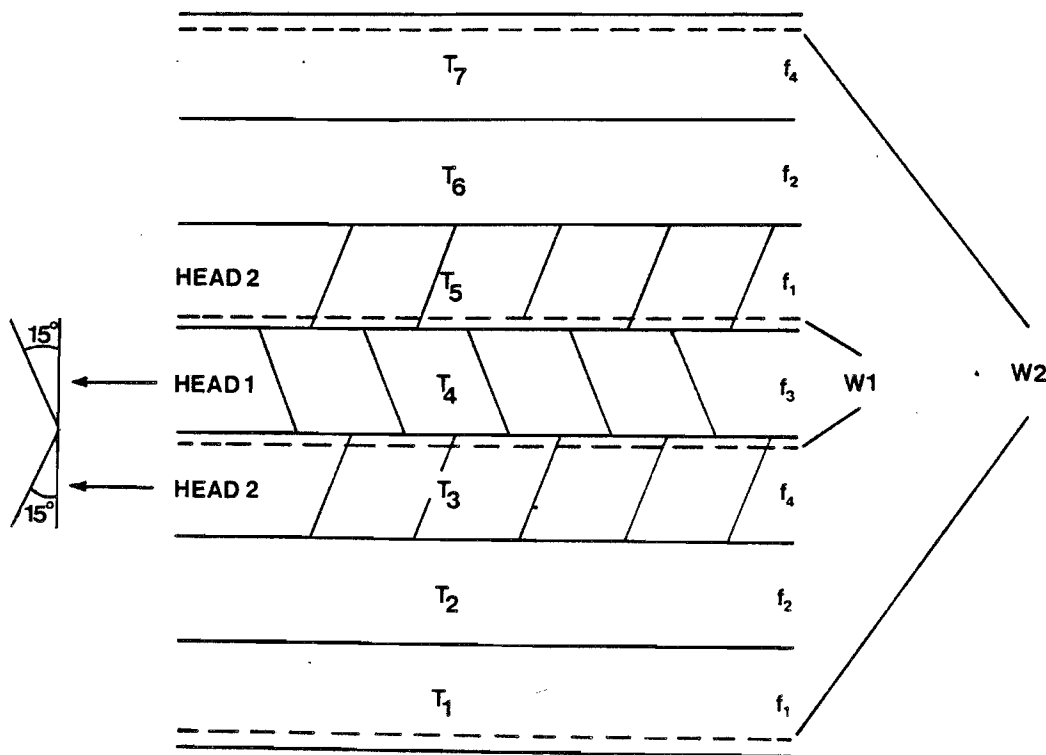
Figure 1.12a

Figure 1.12b

Near the gap $|x| < 20$ µm we see that the width (W_1) of the head is 23 µm. For increasing $|x|$ the width of the gap increases and for $|x| > 60$ micrometer even more strongly. The reason for this is illustrated in Figure 1.12b. Supposing that T_4 is the actual track and T_3 and T_5 are its neighbours, it can be seen that the low frequencies of T_1 and T_7 can disturb the tracking process, unless they are read with a gap length that suppresses even these low frequencies.

Heads of the kind of the one illustrated in Figure 1.12a are used in the Philips V2000 recorder. In fact two heads are used, that write a track in turn. They have different azimuth as shown in Figure 1.12b. This results in an extra attenuation of the high frequency crosstalk of adjacent tracks due to mistracking, because it is read with a head that is 30° out of line. For long wavelengths the crosstalk is of far less importance. That is why we neglect it and take the gap perpendicular to the x-axis.

The head we used in our calculations (Figure 1.13 and 1.14) has two planes of symmetry (x=0 and z=0) instead of one (x=0). Furthermore it has a flat pole-face instead of a

curved one. In this way the input for the program package
PADDY is considerably simplified and we still have the real
situation of a head pressed against the tape. The sizes of
the head are slightly different as those in Figure 1.12a, but
a comparison with former results (Van de Berg, 1981) is pos-
sible now.

VIDEO HEAD

DIMENSIONS IN MICROMETERS

POLE-FACE

| 217 |

FRONT VIEW

CROSS-SECTIONAL VIEW

128.5

400   820

800

3000

-200-

3000

Figure 1.13

8222 256 95021
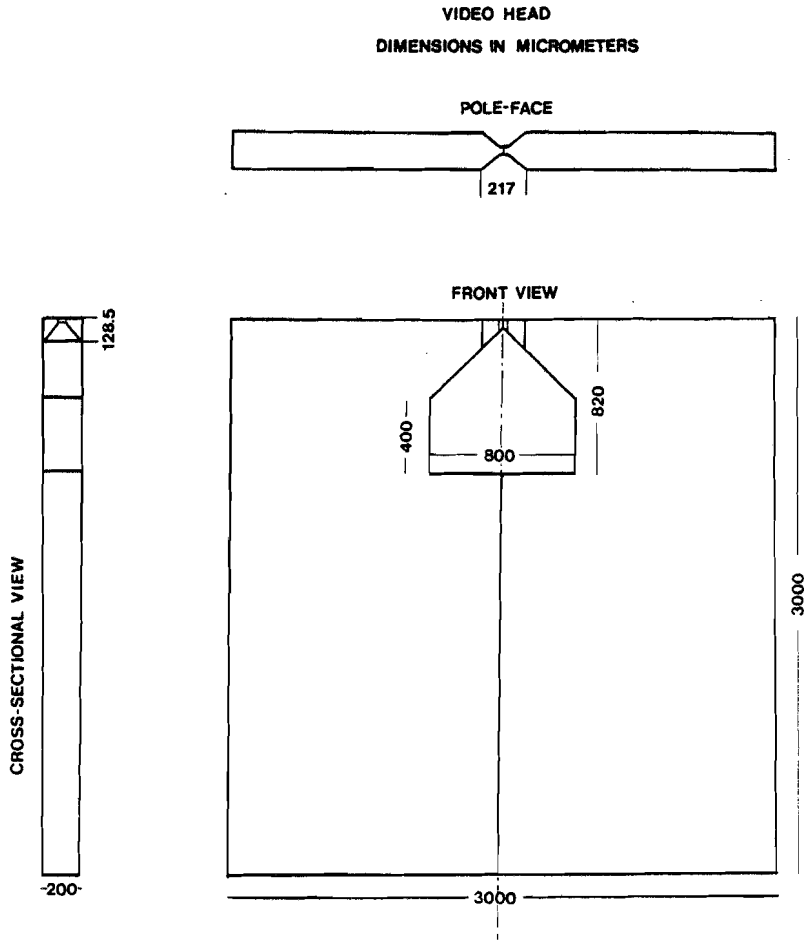
Figure 1.14
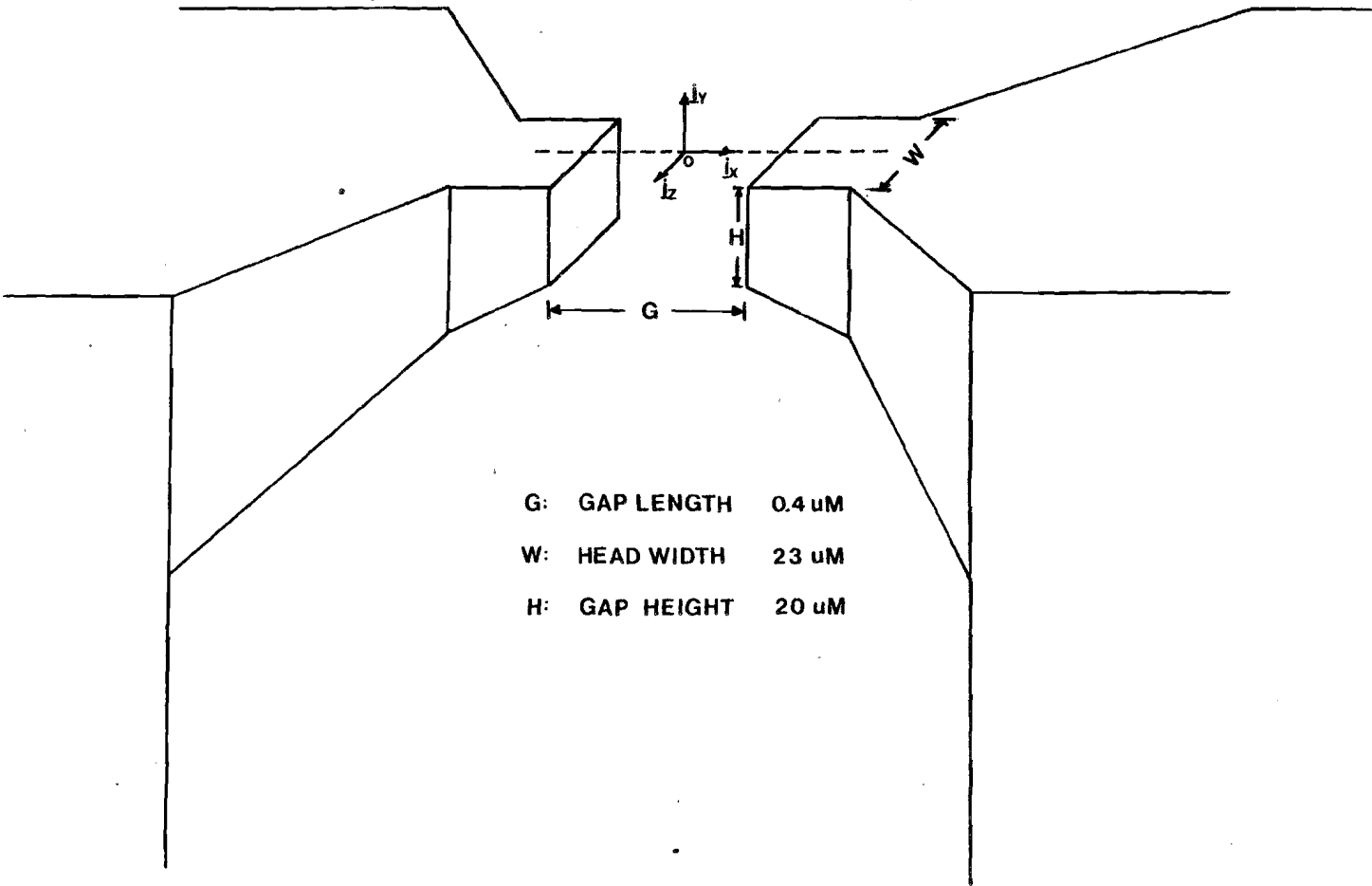
G: GAP LENGTH   0.4 uM

W: HEAD WIDTH   23 uM

H: GAP HEIGHT   20 uM

1.4. SOME RESULTS OF MAGNETIC RECORDING THEORY

In this section we give some results of magnetic recording theory and define most of the quantities we use. Throughout this report SI units are used.

In paragraph 1.1. we mentioned the constant velocity which the medium should be moved with past the head. This velocity v (m/sec) is related to the recorded wavelength λ (m) and the frequency f (1/sec) of the signal as given by:

$$v = \lambda \cdot f \qquad\qquad 1.3$$

The wave number k is defined by:

$$k = 2\pi / \lambda \qquad\qquad 1.4$$

In the following we will use two Fourier transforms:

a) time (t)   frequency (ω)
b) space (x)   wavelength (λ)

The transform pairs related to a) and b) are:

$$\tilde{f}(\omega) = \int_{-\infty}^{\infty} f(t) e^{j\omega t} dt \; ; \; f(t) = \frac{1}{2\pi} \int_{-\infty}^{\infty} \tilde{f}(\omega) e^{-j\omega t} d\omega \qquad 1.5a$$

$$\tilde{f}(k) = \int_{-\infty}^{\infty} f(x) e^{jkx} dx \; ; \; f(x) = \frac{1}{2\pi} \int_{-\infty}^{\infty} \tilde{f}(k) e^{-jkx} dk \qquad 1.5b$$

$\tilde{e}_R(\omega)$, the Fourier Transform of the read voltage $e_R(t)$, is called the harmonic response of a magnetic head. Since

1.1. is an expression for the read voltage, we can write for the harmonic response

$$\tilde{\ell}_R(\omega) = j\omega\tilde{\tilde{\phi}}(\omega) \qquad (n=1) \qquad 1.6$$

An expression for $\phi(t)$ is given by the reciprocity theorem of magnetic recording theory (De Hoop, 1977):

$$\phi(t) = \mu_0 \iiint_V \underline{H}(\underline{r}) \cdot \underline{M}(\underline{r},t) \, dV \qquad 1.7$$

where:

$V \quad (m^3)$ domain occupied by the recording head

$\underline{H}(\underline{r}) \quad (A/m)$ head field obtained by a current of 1A through the head's coil in the absence of the tape

$\underline{M}(\underline{r},t) \quad (A/m)$ magnetization of the medium defined by $\underline{M}=(\underline{B}/\mu_0)-\underline{H}$, where $\underline{B}$ is the magnetic induction in Tesla (T).

It is possible to derive an expression for $\tilde{\tilde{\phi}}(\omega)$ (Van Herk, 1980):

$$\tilde{\tilde{\phi}}(\omega) = \mu_0 \iint_A \underline{\tilde{M}}(-k;y,z) \cdot \underline{\tilde{H}}(k;y,z) \, dA \qquad 1.8$$

where

$A \quad (m^2)$ the cross section of the medium perpendicular to the direction of transportation

$\underline{\tilde{M}}(k;y,z)$ and $\underline{\tilde{H}}(k;y,z)$ are the Fourier transforms of $\underline{M}(r,t)$ and $\underline{H}(r)$ respectively.

H(k;y,z) is called the harmonic flux sensitivity function of

the head. The flux sensitivities for the longitudinal and perpendicular components of M are then given by $\widetilde{H}_x(k;y,z)$ and $\widetilde{H}_y(k;y,z)$ respectively.

On the basis of the behaviour of the <u>static</u> magnetic field at the edges of a head and of the sensitivity functions, statements can be made about the crosstalk (Luitjens, Van Herk; 1982). Throughout this report cross talk has our major interest, therefore much attention is payed at the interpretation of the magnetic field and its Fourier transform.

Both the calculation of the field and the sensitivity function have to be done numerically. In chapter two we propose a model for the video head, to study the cross talk.

CHAPTER TWO

A THREE-DIMENSIONAL ANALYTICAL MODEL FOR THE EFFECT OF THE CONSTRICTION

2.0. INTRODUCTION

2.1. A THREE-DIMENSIONAL ANALYTICAL MODEL FOR THE GAP-FRINGING FIELD OF A RING HEAD

2.2. A MODEL FOR THE EFFECT OF THE CONSTRICTION

PHILIPS

2.0. INTRODUCTION

In this chapter we start with an analytical model for a ring head. The necessary theory is treated and the results are compared with the ones found in literature. The second paragraph deals with the analytical model for <u>the effect of the constriction</u>. Results, related to a real situation, are presented and discussed.

8222 256 95021

2.1. A THREE-DIMENSIONAL ANALYTICAL MODEL FOR THE GAP-FRINGING FIELD OF A RING HEAD

The model described is an analytical one and therefore has the advantage, that the results can be computed easily. The fact that it is three dimensional, offers us the possibility to study the crosstalk effect. To explain the model, we have to treat some theory first.

We suppose that the ring head consists of a soft-magnetic body excited by a current carying coil (write process) and positioned in free space. The near gap field is considered to be caused by the magnetization of the head only. This is justified by the fact that, near the gap, the contribution of the field of the current carrying coil is neglectable. In this way the problem is restricted to a magnetostatic one without currents. Problems of this kind can be described with the following equations of Maxwell.

$$\nabla \times \underline{H} = \underline{0} \qquad\qquad 2.1$$

$$\nabla \cdot \underline{B} = 0 \qquad\qquad 2.2$$

Furthermore we have:

$$\underline{B} = \mu_0 \left(\underline{H} + \underline{M} \right) \qquad\qquad 2.3$$

The vector $\underline{B}$ is called the magnetic induction (Tesla). The quantity μ_0 is the magnetic pressurability of the vacuum. V is the bounded domain in space occupied by the head, the boundary surface of the head is called S. On S 2.1. and 2.2. should be supplemented with the boundary conditions: $\underline{n}\times\underline{H}$ and $\underline{n}.\underline{B}$ continuous when crossing S.$\underline{n}$ is the unit vector along the normal on S in the outward direction.

However we are interested in the field outside the head at the position of the tape. For this we take the right-handed system of Figure 1.14. The position vector of the observer is called $\underline{r}$ and the position vector of a point on the

surface of the head: $\underline{r}$.

From 2.1. and 2.2. it follows that we may write:

$$\underline{H}(\underline{r}) = -\nabla_{\underline{r}}\, U(\underline{r}) \qquad\qquad 2.4$$

with

$$U(\underline{r}) = \iiint\limits_{V(\underline{r}')} -\nabla_{\underline{r}'}\cdot M(\underline{r}')\, G(\underline{r},\underline{r}')\, dV(\underline{r}') \;+\;$$

$$\oiint\limits_{S(\underline{r}')} \underline{n}\cdot M(\underline{r}')\, G(\underline{r},\underline{r}')\, dS(\underline{r}') \qquad\qquad 2.5$$

Furthermore we define the free-space Green function:

$$G(\underline{r},\underline{r}') = \frac{1}{4\pi|\underline{r}-\underline{r}'|} \qquad\qquad 2.6$$

For the case of a magnetic material with a high μ_r the magnetic potential $U(\underline{r})$ changes significantly only on crossing the gap. Now an approximation for the field near the gap can be given by the field of two homogeneously charged quadrangler of opposite sign at the inner faces of the gap of the ring head. These two sheets represent the potential jump on crossing the gap in the direction of transportation (positive x-direction, Figure 2.1).
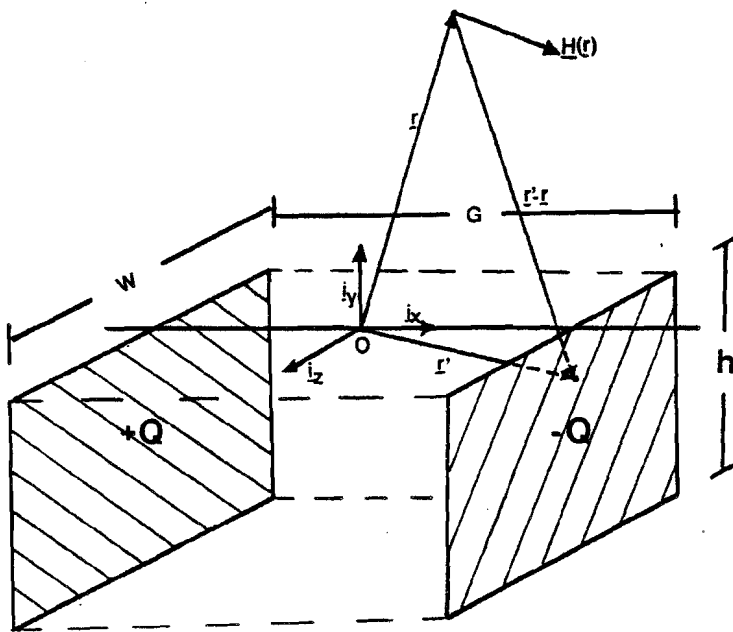
G≪H , G≪W (Figure 1.14)

Figure 2.1

As mentioned earlier the model is three-dimensional. This is
an advantage with respect to the two-dimensional models of
Westwijze (1953) and Karlqvist (1954). A disadvantage how-
ever is, that the field does not satisfy the real boundary
conditions on the pole-face near the gap. Despite this dis-
advantage the model has been used successfully by McCary
(1971) and Chi (1974) for a ring head. Luitjens and Van Herk
(1982) used the model to approximate a single pole head
(perpendicular recording).

An expression for the field of a plane <u>triangularly</u>
<u>shaped</u> distribution of magnetic charge with linearly varying
density can be found in Van Herk (1980). In our case we need
an expression for a <u>quadrangularly shaped</u> distribution $A(\underline{r}')$
of magnetic charge with a constant density $\sigma_M(\underline{n}.\underline{M}(\underline{r}'))$

$$\underline{H}(\underline{r}) = \nabla_M \iint_{A(\underline{r}')} \nabla' G(\underline{r}, \underline{r}') \, dA(\underline{r}') \qquad 2.7$$

The integral in 2.7 is tackled by a fully vectorial analysis. As a result the plane of the quadrangle A can take any position with regard to the coordinate system.

$$\underline{H}_A(\underline{r}) = \frac{-\nabla_M}{4\pi} \left\{ \left(\sum_{m=1}^{4} (\underline{n}_Q \times \underline{t}_m) L_m \right) + \underline{n}_Q \, \Omega \right\} \qquad 2.8$$

where

$$L_m = \ln \left(\frac{a_m \cdot \rho_{m+1} + a_m \rho_{m+1}}{a_m \cdot \rho_m + a_m \rho_m} \right) \qquad 2.9$$

$$\Omega = \iint_{A(\underline{r}')} \underline{n} \cdot \nabla' G(\underline{r}, \underline{r}') \, dA(\underline{r}') = -\iint_{A(\underline{r}')} \frac{\underline{n} \cdot (\underline{r}' - \underline{r})}{|\underline{r} - \underline{r}'|} \, dA(\underline{r}') \qquad 2.10$$

The other symbols used, are defined in Table 2.1:

$\underline{r}_m$	position vectors of the vertices
$\underline{a}_m$	vectorial sides of the quadrangle $\underline{a}_m = \underline{r}_{m+1} - \underline{r}_m$
$\underline{\rho}_m$	vectors from the point of observation r to the vertices $\underline{\rho}_m = \underline{r}_m - \underline{r}$
$\underline{t}_m$	unit vectors along the tangents to the sides of the quadrangle
$\underline{n}_Q$	unit vector along the normal on the quadrangle, the direction of circulation along the boundary contour C of the quadrangle forms a right-handed system with $\underline{n}$ (Figure 2.3)
a_m	$|\underline{a}_m|$ etc.

Table 2.1

Figure 2.2

Ω is the signed solid angle at which the quadrangle is observed from the point of observation. Ω is negative when the point of observation r is at the same side of the quadrangle as to where $\underline{n}_0$ points and is positive in the other case.

Figure 2.3

The derivation of 2.8 is given in appendix A.

We now have an analytical expression for the magnetic field of a plane homogeneously charged quadrangle, that can be calculated numerically. Our model of the ring head consists of two quadrangles of opposite charge. So, the total field can be obtained by super position of the fields of each of the quadrangles separately. This model has been implemented on the computer and the results shown in Figure 2.4. Since we are interested in the near edge field at the position of the tape, we made 3D-plots of the field components in the plane: $y=0.1$ μm above the head.

FIELD COMPONENTS OF THE RING HEAD MODEL   Y=0.1uM
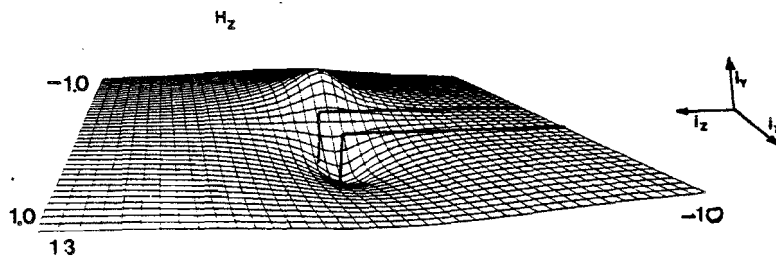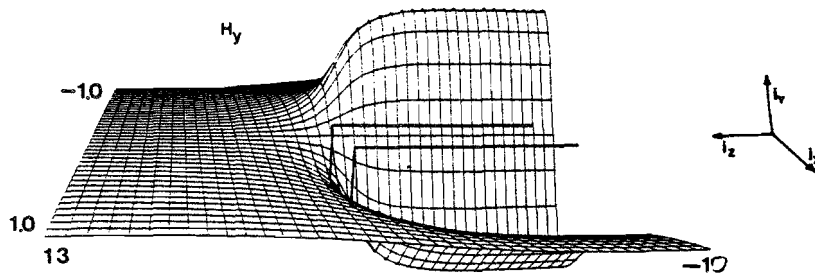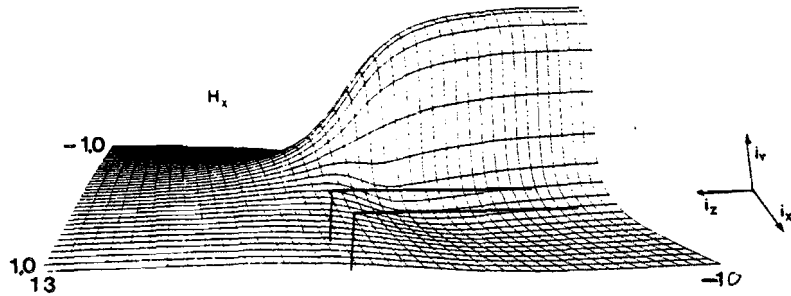
dimensions in μM

Figure 2.4

Looking at these results, the following points strike us:

- In contrast to Hx, Hy and Hz show an asymmetrical beha-
  viour near the gap.

- Hx has a maximum at the position of the gap (x=0), it de-
  creases for increasing y (not shown here).

- Hy is zero at the position of the gap (x=0) and reaches
  extrema on both sides of the gap. These extrema decrease
  and withdraw from the gap for increasing y (not shown
  here).

- In this configuration and at y=0.1 μm Hz differs signifi-
  cantly from zero only near the edge and even there it is
  much smaller than Hx and Hy.

- Although the maximum of |Hy| is smaller than the maximum
  of Hx, it can be clearly seen, that the maximum of |Hy|
  decreases faster than the maximum of Hx for constant y and
  increa-sing z. As a consequence in the perpendicular mode
  there will be less side writing than in the longitudinal
  recording mode (Figure 1.4).

To study the crosstalk phenomenon we calculated the
Fourier transform (1.5b) of the magnetic field to obtain the
sensitivity function $|\tilde{H}_x(k;y,z)|$ and $|\tilde{H}_y(k;y,z)|$. This calcula-
tion has been carried out in the plane y=0.1 μm at z=0.0,
12.0 and 20.0 μm respectively. The results are given in
Figure 2.5.

SENSITIVITY FUNCTIONS   RING HEAD MODEL
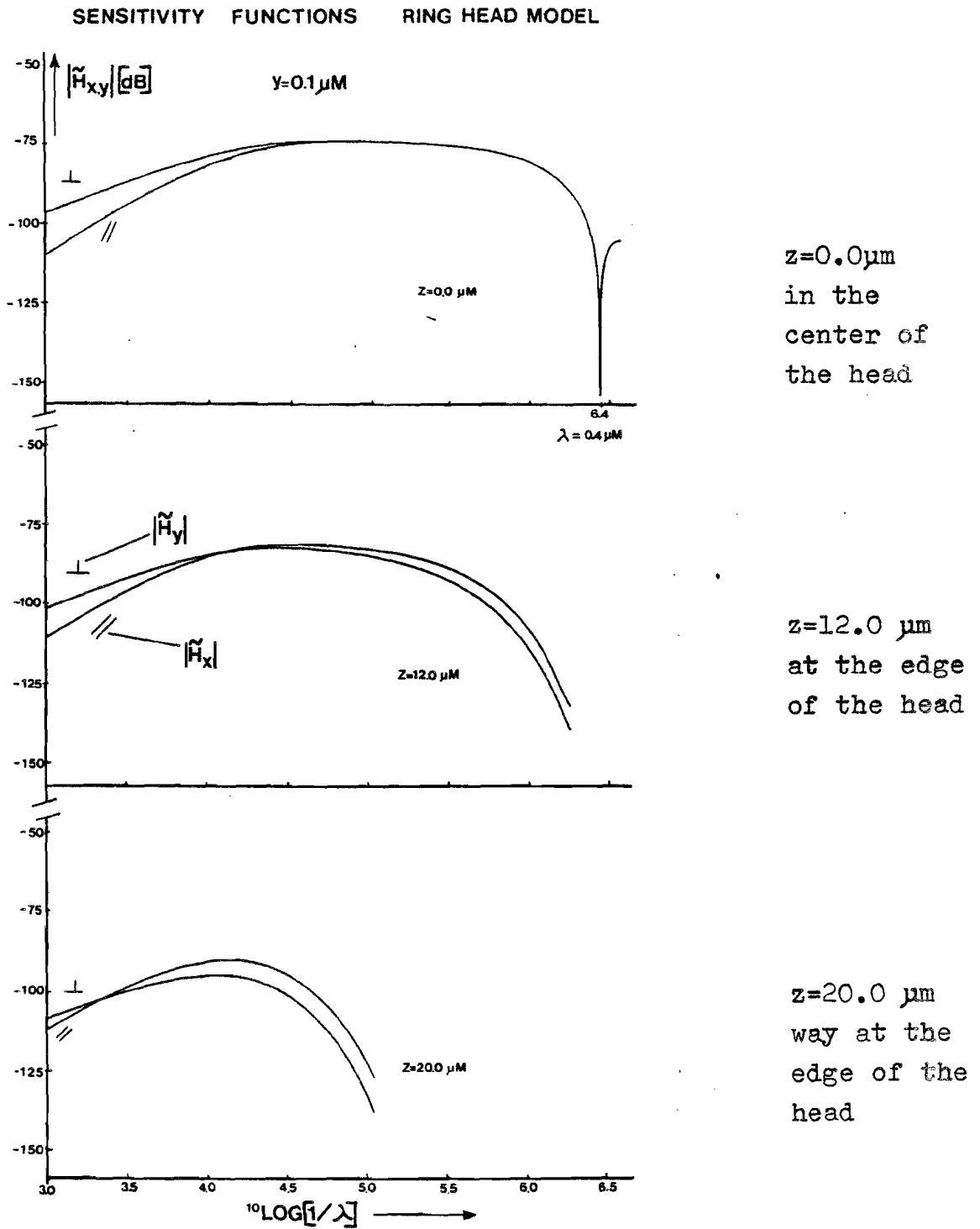
Figure 2.5

For very large wavelengths and for very small wavelengths the numerical calculation of the Fourier Transform gives unreliable solutions, but these wavelengths are of no importance for video recording, so they are left out in this report.

In Figure 2.5 we notice that in the region <u>above the head</u>: $|z| \leq (1/2)W$ (Fig. 2.1):

- first dip at $\lambda = 0.4$ μm;

- in the plane of symmetry z=0.0 and for $\lambda < 32$ μm $|\tilde{H}_x| = |\tilde{H}_y|$; for z-values near the edges the equality disappears for smaller wavelengths;

- for increasing y the equality disappears also for smaller wavelengths (not shown here).

In the region <u>beside the head</u> $|z| > 1/2$ W:

- The values of $|\tilde{H}_x|$ and $|\tilde{H}_y|$ are different for all wavelengths;

- for small wavelengths the longitudinal sensitivity function has larger values than the perpendicular one.

So in spite of the fact that this two plate model does not take into account the effect of the correct boundary conditions at the head, we find the first dip at exactly the gap length. In the symmetry plane x=0 the two-dimensional approach is valid for small wavelengths because $|H_x|$ and $|H_y|$ are equal and this is a property of two-dimensional head configurations (Appendix B). For large λ-values the three-dimensional character of the head becomes evident. The same is noticed for increasing y. As far as crosstalk is concerned, we find that the longitudinal recording mode is more sensible for crosstalk than the perpendicular mode (for small wavelengths). Analogous results are found by Luitjens and Van Herk (1982) with their "cubical head".

Stratton (1941) states that at larger distances the field of a magnetic source approached the field of a corresponding dipole. Similar to mechanics a dipole moment $\underline{m}_d$ and a geometrical point of gravity: $\underline{r}_d$ can be defined

$$\underline{m}_d = \iiint_{V_M(\underline{r}')} \rho_M(\underline{r}')\, \underline{r}'\, dV(\underline{r}') \qquad 2.11$$

$$\underline{r}_d = \frac{\iiint_{V(\underline{r}')} \underline{r}'\, dV(\underline{r}')}{\iiint_{V(\underline{r}')} dV(\underline{r}')} \qquad 2.12$$

where $V(\underline{r}')$ is the volume of the magnetic source involved and $\rho(\underline{r}')$ the volume charge density. In our case we have a longitudinal dipole $\underline{m}_d = -V_M A i_x$ and $\underline{r}_d = (0, -1/2H, 0)$ pointing in the negative x-direction (Figure 2.1). For the sensitivity functions $\tilde{H}_{dx}$ and $\tilde{H}_{dy}$ analytical expressions exist (Van Herk, 1980). In our problem they reduce to:

$$\tilde{H}_{dx}(k;y,z) = (2\pi a^2)^{-1}\left[m_x\, 2ak\, K_1(ak) - (ak)^2 K_2(ak)\right] \qquad 2.18$$

$$\tilde{H}_{dy}(k;y,z) = (2\pi a^2)^{-1}\left[j m_x (ak)^2 \frac{y}{a} K_1(ak)\right] \qquad 2.19$$

where K_1 and K_2 are modified Bessel functions of the second kind. Furthermore the following expression holds (Abramowitz, 1964)

$$K_o(ak) = K_2(ak) - \frac{2K_1(ak)}{ak} \qquad 2.20$$

$$a = \sqrt{(y - z_{dy})^2 + (z - z_{dz})^2} \qquad 2.21$$

It is interesting now to compare the behaviour of the
F.T. of the dipole field with that of the field of the ring
head model for large wavelengths. The sensitivity functions
for the dipole are plotted in Figure 2.6. Examining these
results we see:

- for all z-values the longitudinal sensitivity functions
  approximate the ones of the ring model for the large wave-
  lengths;
- the perpendicular sensitivity function of the dipole has
  larger values than the corresponding one of the ring head
  model, this difference decreases for increasing z-values.

The results above indicate that a ring head in three
dimensional space, at least the perpendicular sensitivity
function cannot always be approximated by the one of a cor-
responding dipole for large wavelengths. Apparently the be-
haviour of the two fields for smaller distances of the head,
causes the sensitivity functions to differ for larger wave-
lengths (Luitjens, Van Herk 1982).
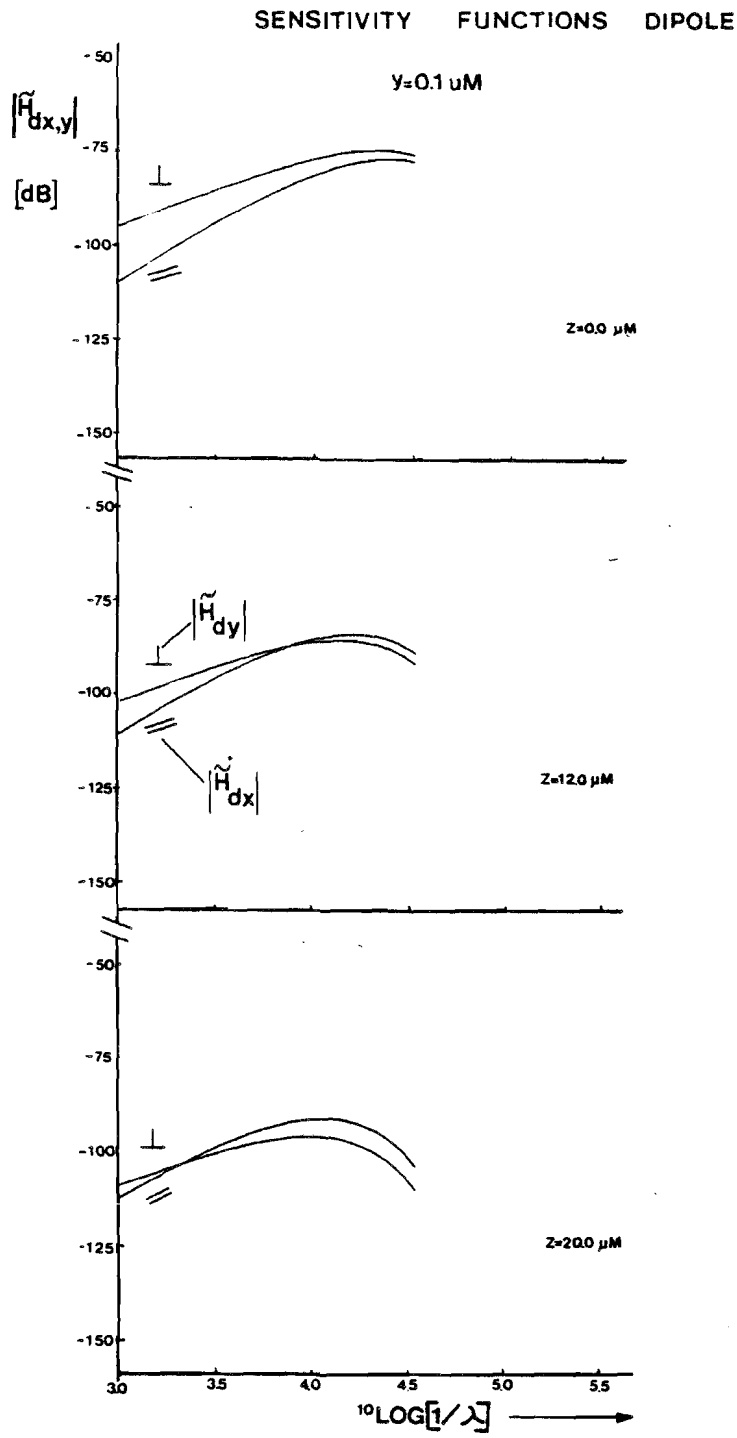
Figure 2.6

2.2. A MODEL FOR THE EFFECT OF THE CONSTRICTION

In section 2.1. we used two homogeneously charged qua-
drangles (of opposite sign) to approximate the near gap
field of a ring head. The dimensions of these quadrangle
and their distance (gap length) were chosen equal to those
of the inner faces of the gap of the video head (Figures
1.14 and 2.1). To approximate the effect of the constriction
in a video head, the number of quadrangles is increased. The
"video head model" consists of the four sloping sides of the
constriction ($-h \leqslant y \leqslant 0$) and the two plates of the ring
head model (Figure 2.7).
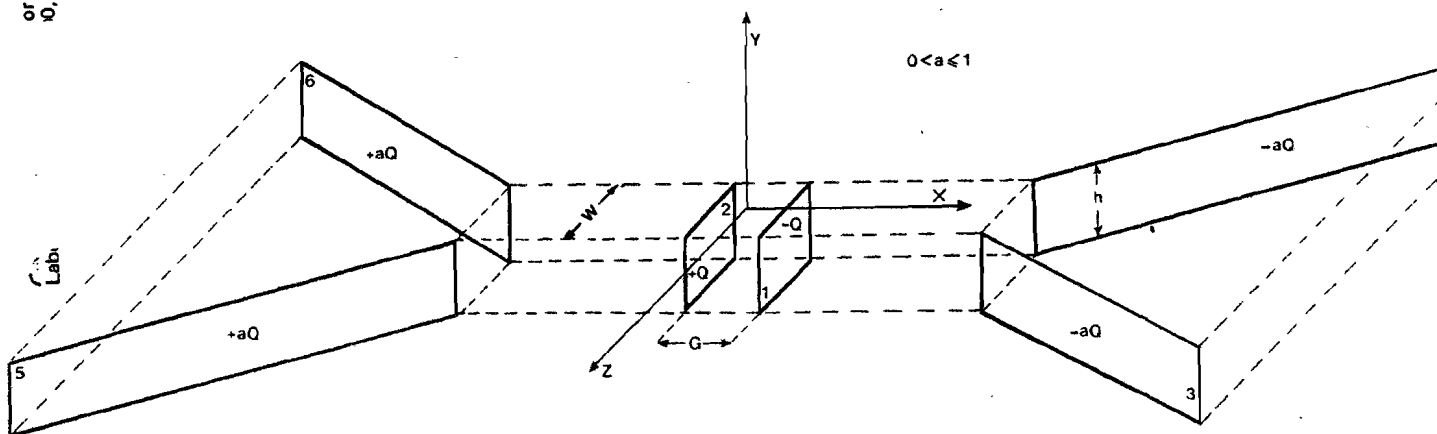
Figure 2.7

It is obvious that in this model, just as in the ring
head model, the boundary conditions at the surface of the
head are not satisfied. Furthermore the charge density ∇M_i
(i=3,....,6) will change as a function of the position on the
corresponding quadrangles. In our model, however, we only
use quadrangler with a constant charge density, so chosing a
value for ∇M_i implies a compromise.

In attaching the ∇M_i's we anticipate on the results
obtained with the program package PADDY (Chapter 3). To ap-
proximate the almost homogeneous gap field calculated with
PADDY ($\underline{H} \approx H_x \underline{i}_x$ and $H_x \approx 1.4 \ 10^5$ A/m, page 62 we take
$|\nabla M_{1,2}| = 1.4 \ 10^5$ A/m. In order to define the $|\nabla M_i|$, the

factor a is chosen such, that the extrema of Hx along the line z=40.0 μm in our model match with the extrema of Hx of the field calculated with PADDY along the same line (a=0.03062, page 62)

The resulting Hx and Hy component are shown as a function of x along lines of constant z value in Figures 2.9 and 2.10 in the plane y=0.25 μm. The z values are:

z=0.0   symmetry plane

z=12.0 μm   near the edge of the gap

z=20.0 μm   way at the edge of the gap

z=40.0 μm   way at the edge of the gap

It should be noted, that in these figures $-100 \ \mu m \leqslant x \leqslant 100 \ \mu m$, while in Section 2.1. Figure 2.4: $-1.0 \ \mu m \leqslant x \leqslant 1.0 \ \mu m$.

In Figure 2.8 the Fourier Transform for corresponding z values at y=0.25 μm of the ring head model are given. The homogeneous gap field corresponds to the one of the video-head model.

SENSITIVITY FUNCTIONS   RING HEAD MODEL IN Y-0.25μM
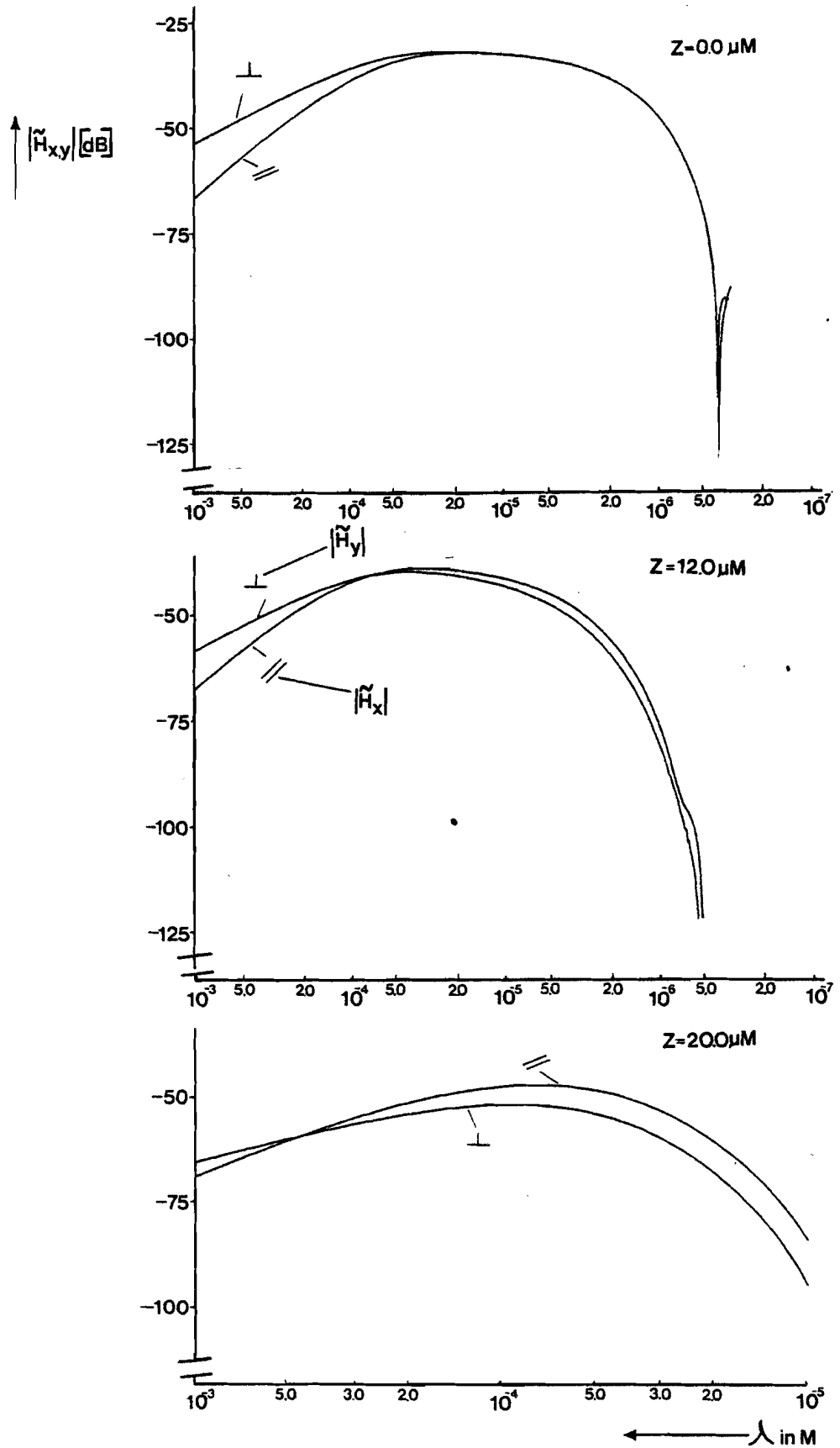
Figure 2.8

H_x COMPONENT OF VIDEO HEAD MODEL
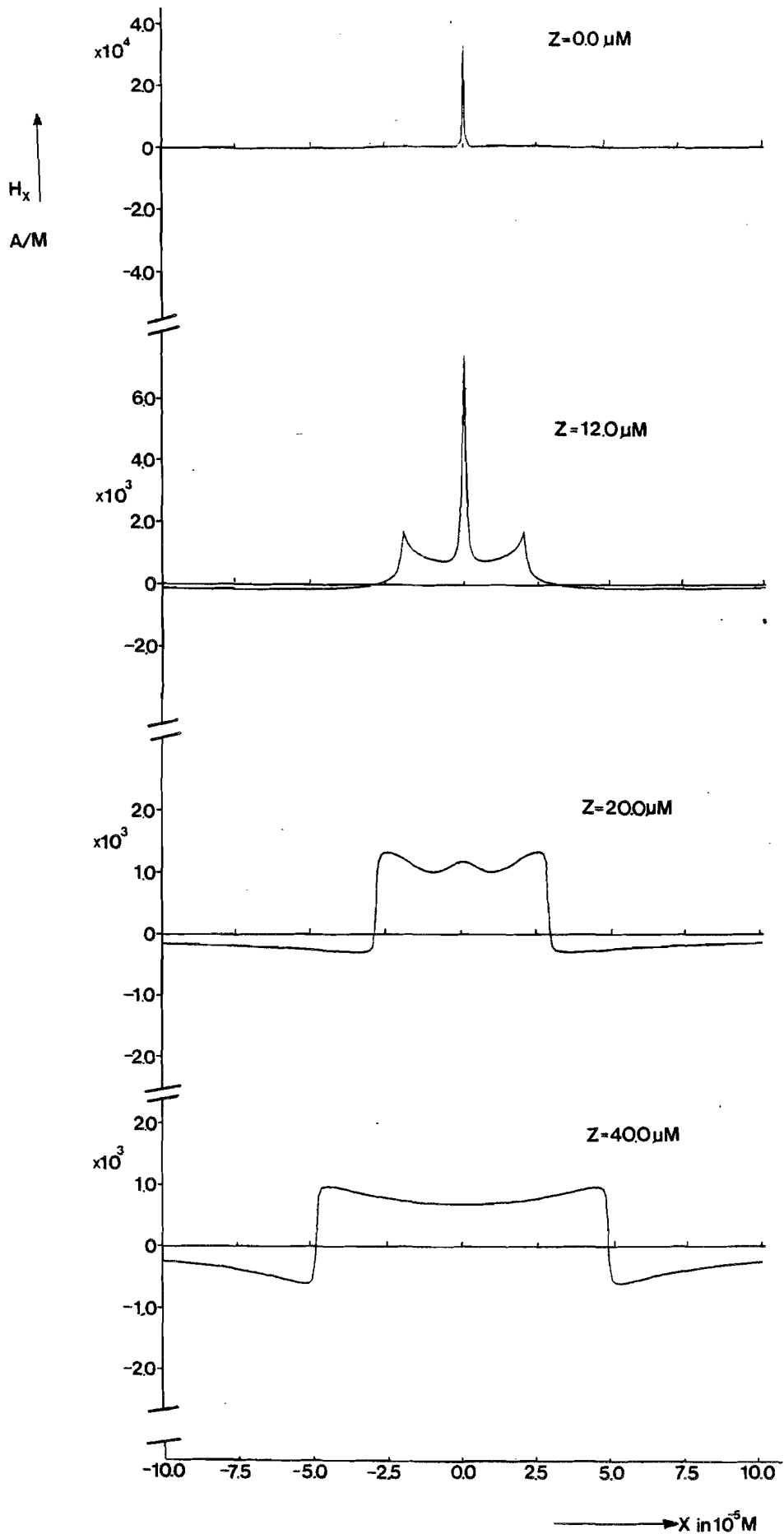
IN Y=0.25 µM

Figure
2.9

Hy COMPONENT OF VIDEO HEAD MODEL

IN Y=0.25μM
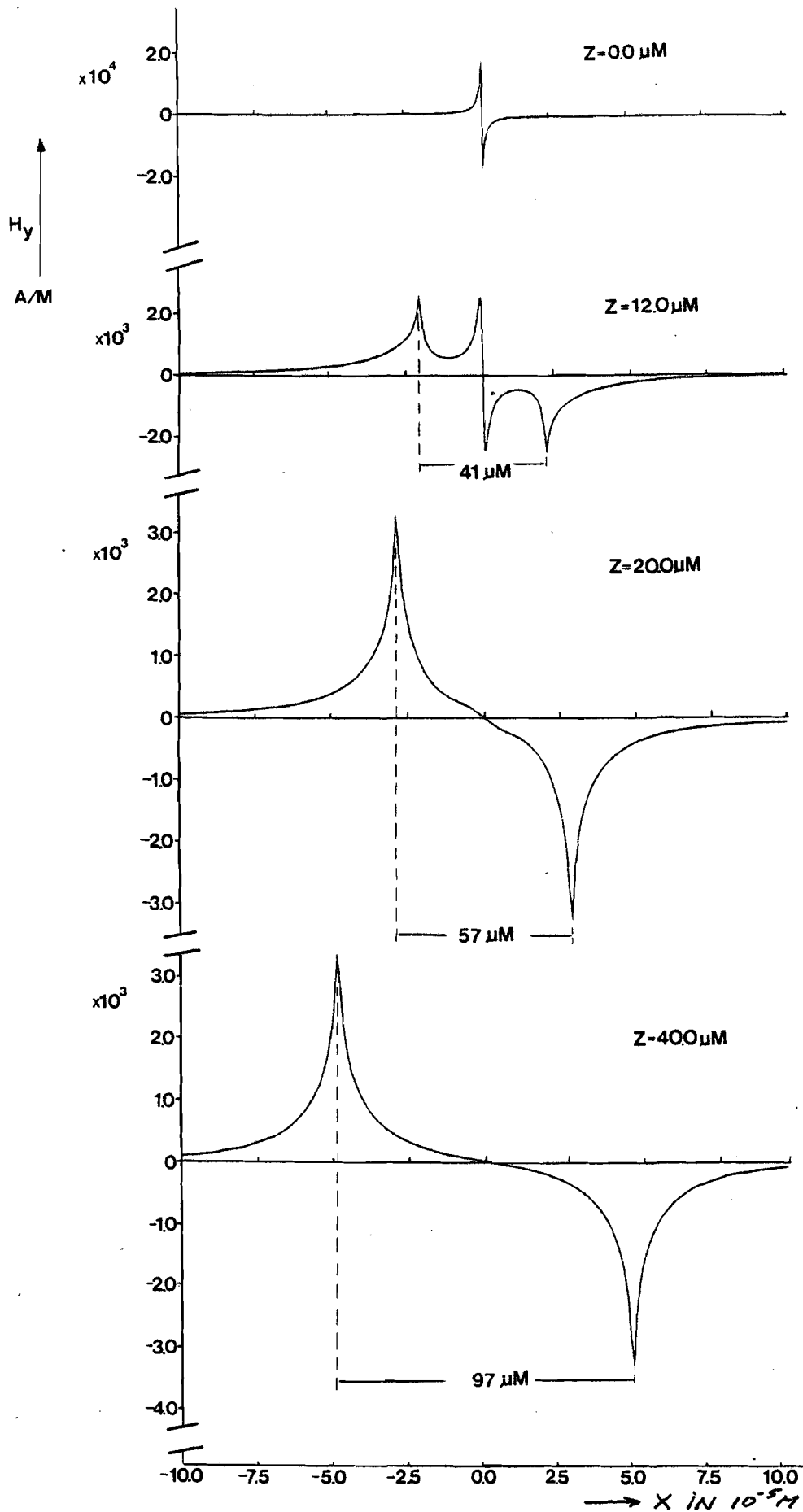
Figure
2.10

In Figures 2.9 and 2.10 we notice:

- In the symmetry plane z=0 the results conform with those
  of Figure 2.8 at $|x|$ =20 µm the influence of the four
  sloping plates can be seen.

- z=12.0 µm: the gap fringing field still dominates.

- z=20.0 µm: the gap fringing is hardly perceptible and the
  field of sloping quadrangles dominates.

- z=40.0 µm: there is only the field due to the sloping
  plates.

- Due to the absence of magnetic material the Hx component
  crosses zero at the position of the plates and the Hy com-
  ponent reaches its extrema there.

    In Figure 2.10 we used the distance between the extrema
of Hy in the x direction to denote the: "secondary gap", due
to the constriction along a line of constant z value. We
will use these in the discussion of the results of the
Fourier Transform of the field components (Figure 2.11).

SENSITIVITY FUNCTIONS   VIDEO HEAD MODEL   IN Y=0.25μM
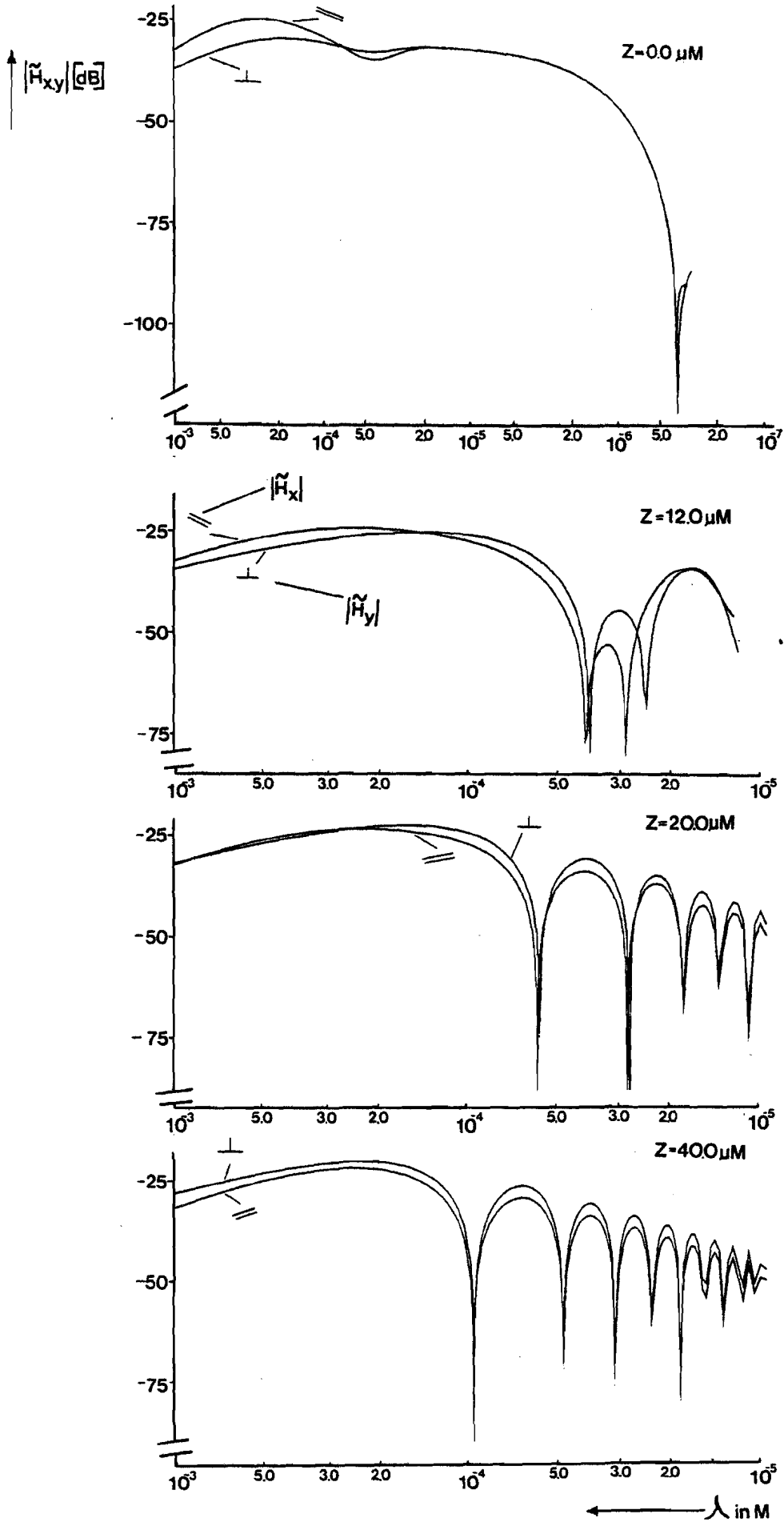
Figure
2.11

Figure 2.11 shows the sensitivity functions $|\tilde{H}x(k;y,z)|$ and $|\tilde{H}y(k;y,z)|$ for the same z values as in Figures 2.9 and 2.10 and for the same plane 0.25 µm.

The following remarks can be made:

- In the symmetry plane z=0 $|Hx|$ and $|Hy|$ are equal for small λ again ($\lambda < 32$ µm) and the influence of the sloping quadrangles results in a small dip ($\lambda \approx 45$ µm). The values for larger wavelengths $\lambda > 100$ µm are larger than in the ring head model.

- z=12.0 µm: the first dips in $|Hx|$ and $|Hy|$ are at $\lambda \approx 39$ µm as expected (Figure 2.10). The other dips do not coincide. This is merely due to the fact, that the gap fringing field is dominating. Furthermore the fact that we are near the edge of plates nr. 3 and nr. 5 contributed.

- z=20.0 µm: the influence of the gap has vanished almost completely. The dips coincide at the expected wavelengths.

- z=40.0 µm the same accounts as for 20 µm.

Compared to the ring head model the sensitivity functions of the video head model have larger values for $|z| > 11.5$ (above the constriction). Within the limitations of this model we conclude that the video frequencies of the neighbouring tracks are suppressed due to the secondary gap effect of the constriction. The suppression starts at about 125 kHz, so some of the track following frequencies would be suppressed too (Figure 1.8a). This is due to the dimensions of the constriction as chosen for this particular model (Figure 1.13).

CHAPTER THREE

PADDY A PROGRAM PACKAGE FOR SOLVING THREE-DIMENSIONAL
MAGNETOSTATIC PROBLEMS.

3.1. FACILITIES OF THE PROGRAM PACKAGE

3.2. THE ALGORITHM BLOCK

3.3. THE PADDY INPUT FOR THE VIDEO HEAD

INTRODUCTION

Chapter three is dedicated to the description of the program package PADDY. Firstly we describe some facilities Then we will treat the specification of the mesh statements. In the last paragraph the input for the video head problem is treated.

In PADDY the solution is calculated in terms of the magnetic potential, using a finite element method. A brief description of the solution method of our own PADDY problem will be given in Appendix C.

3.1. FACILITIES OF THE PROGRAM PACKAGE

Paddy offers facilities for the approximate solution of
three dimensional static problems. It is primarily meant for
magnetic fields but can equally well be used for electrosta-
tics or with some restrictions for heat distribution (De
Beer, 1981).

A magnetic problem may contain soft isotropic materials
or hard anisotropic materials, static currents and air. The
sources may be permanent magnets, currents, boundary poten-
tials or imposed fluxes.

The basic quantities involved are

$\underline{H}$ magnetic field strength (A/M)

$\underline{B}$ magnetic induction (Tesla: T)

U magnetic potential (scalar) (A)

$\underline{J}$ static current density (A/m^2).

Maxwell's equation for magnetostatic problems are :

$$\nabla \times \underline{H} = \underline{J} \qquad\qquad 3.1$$

$$\nabla \cdot \underline{B} = 0 \qquad\qquad 3.2$$

The vectors $\underline{B}$ and $\underline{H}$ are related by

$$\underline{B} = \mu_0 \mu_r (\underline{H}) \underline{H} + \underline{B}_r \qquad\qquad 3.3$$

where $\mu_0 = 4\pi \cdot 10^{-7}$ Vsec/Am and $\underline{B}_r$ is the remanent induc-
tion.

We will restrict ourselves to problems with materials that
have a constant μ_r.

The basic quantity in PADDY is the scalar potential U.
The solution U of the problem is approximated using the fi-
nite element method. In our case this method leads to a sys-
tem of linear equations, which can be solved numerically.

The way this system is achieved, will be described in Appendix C: The mathematical formulation. The numerical solution of the system is not treated.

The general structure of the PADDY package is shown in Figure 3.1.
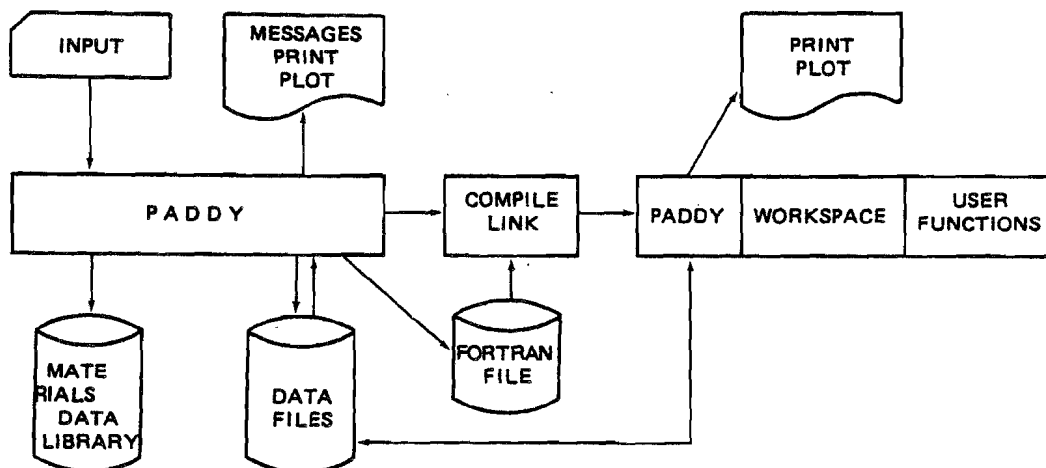
Figure 3.1

The input can be given in the problemoriented language PADLAN (De Beer, 1981). Input for PADDY is always screend for errors by the interpreter part and a transformed form is put on data files. If user - chosen functions are found or if the program needs extra workspace to do the calculations, a few liner of FORTRAN are generated and put on the FORTRAN file (PADDY is completely written in FORTRAN).

When this file has not been generated, processing continues immediately, otherwise the file is compiled first and linked to the existing program, after which processing is resumed. The user has access to a B-H curve library and to the computed values of PADDY for the calculation of secondary results.

As stated in Appendix C, the program package computer the magnetic potential U in certain points in a finite domain a space, specified by the user. Even in a finite part of space, the number of points can take large values. In our

problem this number is about 2.10^4. So in PADDY much attention is paid to simplifying the designation of these so-called nodes.

By connecting all points one gets a mesh and this in fact is the way, the definition of the nodes takes place. In this mesh broken surfaces can be noticed, which are called: "mesh planes". In the input of the problem the user defines these meshplanes by means of mesh statements (section 3.2).

A problem-oriented language PADLAN has been developed to define the problem.
PADLAN offers the possibility to distinguish the input into different sorts of information. We can distinguish in the input:
- information about the mesh;
- information about the structure and the kind of materials and sources used;
- information about the desired output.

In PADDY these parts are called: "blocks" each block has its own identifier. The most important are :

- ALGORITHM   : the mesh of the finite part of free space is defined.

- REGION   : the structure and the dimensions of materials are distinguished. For each material a specific REGION block should be given, the same accounts for the magnetic sources

- PRINT/PLOT : information on the results, that should be printed and/or plotted can be given in this block.

- FORTRAN   : user-chosen function names can be defined. Even user written subroutines to enable post-processing of the results may be declared.

PHILIPS

In the next paragraph special attention is payed at the ALGORITHMblock.

5895

3.2. THE ALGORITHM BLOCK

A magnetostatic problem consists of magnetic materials, currents and air. The air actually extends to infintiy. However as described before, the problem is restricted to a finite domain. The magnitude of this domain is adapated to the accuracy requirements for the far field (De Beer 1981).

In order to specify the nodes in which the potential should be calculated, the mesh planes are defined in the ALGORITHM block of the input. The basic element which the mesh is built from, is the hexahedron, which can be looked upon as a distorted cube (Figure 3.2)
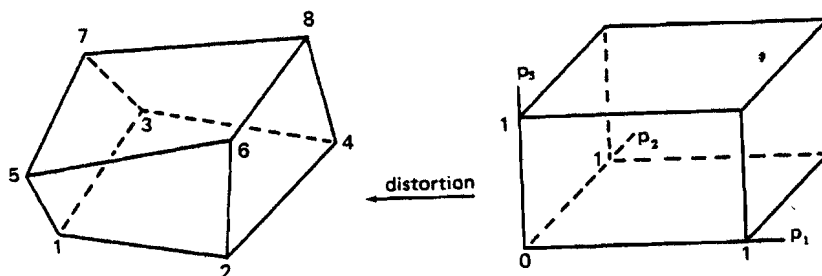
Figure 3.2

On such an element the solution is approximated in a so-called isoparametric way; specifically, the function is trilineair on the cube, and taken through the same distortion as the element shape itself (Appendix C).

Al-ong an edge this results in a linear function of the magnetic potential. Consequently the field component along that edge cannot vary, since $\underline{H} = -\underline{\nabla} U$ (Appendix C). The size of the elements thus determines the accuracy with which the true solution can be approximated. Experience will have to guide the user in his choice.

As stated before, in the assembly of elements one can distinguish what we will call mesh planes. If one connects the topsides of all right, left, front and back neighbour elements, a broken surface with all the element tops as facets is obtained. In a similar way the mesh planes of the other two directions can be defined. The outer boundaries of the problem should be defined by such mesh planes. Obviously there must be six of these. The consequence is that each mesh plane in one direction contains the same number of element sides. The mesh must be laid out such, that all boundaries of materials and sources consist of sides of elements.

In PADDY one can use cartesian, cylindrical or spherical coordinates. We will only treat the mesh specification in cartexian coordiantes. So the above mentioned three directions are the x, y and z direction in this frame.

To define a mesh plane one has to use mesh statements. The simplest case is when a mesh plane

is also a coordinate plane. For the case of the z-coordinate the mesh statement would be

$$Z(A) = B \qquad\qquad 3.4$$

where A is the number of the plane and B is the value of the Z-coordinate.

A more general form of the mesh statement is necessary if the mesh plane is not a coordinate plane. Now the mesh plane is defined by giving the mesh lines in its. A mesh line is the interaction of two mesh planer. When we start in an recoordinate plane, e.g.:

$$X(C) = D \qquad\qquad 3.5$$

8222 256 95021

The specification of a mesh line for the z-coordinate is given by:

$$Z(C, *, F) = E \qquad 3.6$$

This statement means: the mesh line is number F out of the set of mesh lines for coordinate z. This line runs in the y direction, indicated by the place of the star, and lies in the x-plane number C (Figure 3.3).
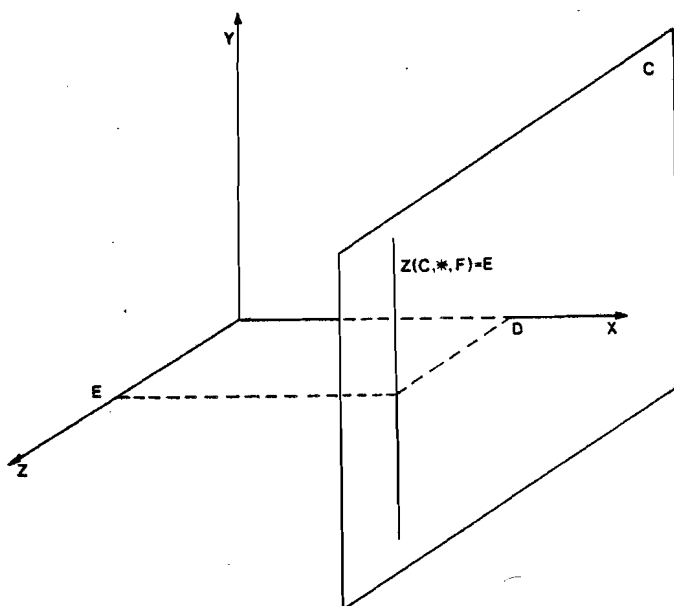
Figure 3.3

Now all z mesh lines have to run in the y-direction. Finally E is the value of the x coordinate in plane c.

On the basis of an example we can show how a broken mesh plane can be achieved. Consider the case that we have 5 x-planes with the numbers 1, 2, 3, 4 and 5 (Figure 3.4); They are coordinate planes, so they can easily be defined with statements X(1) = p , X(2) = q   X(3) = r etc. Now the

PHILIPS

z lines can be specified with

$$Z(1, *, A) = F_1$$
$$Z(2, *, A) = F_1$$
$$Z(3, *, A) = F_2$$
$$Z(4, *, A) = F_2$$
$$Z(5, *, A) = F_2$$

3.7
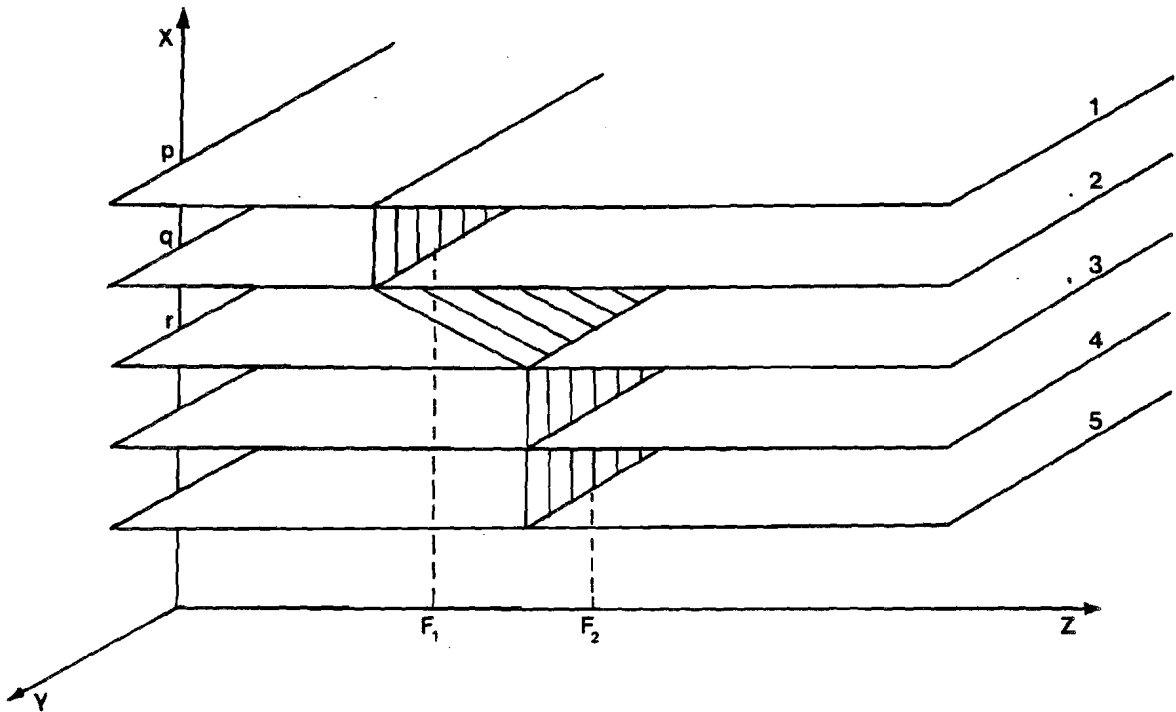
Figure 3.4

Or shorter

$$Z(1:2, *, A) = F_1$$
$$Z(3:5, *, A) = F_2$$

3.8

In figure 3.4 it can be seen that out of a set of z-lines with the same number $(A)_1$ a flat plane $(F_1=F_2)$ or a broken one can arise $(F_1 \neq F_2)$.

All the mesh statements together result in a set of broken planes and/or coordinate planes. If the mesh number of

succeeding planes in the mesh definition is raised with more than one, PADDY specifes the intermediate planes by means of the interpolation (Figure 3.5).
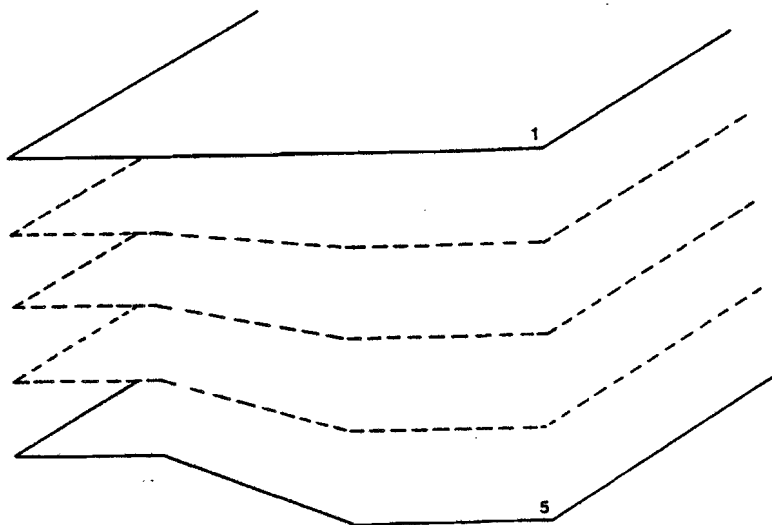
Figure 3.5

The regular pattern of the mesh system implies, that, if in some area a rather fine mesh is needed to obtain a reliable field (near the gap of the video head). The same number of elements must be used throughout, giving use to very many unknown values, that have to be calculated. In order to avoid this effect, it is allowed to have elements without volume. By making their sides coincide the interior dissapears. It will be obvious, that at the point where voluminous and collapsed elements meet, other than hexahedral elements are found.

Despite the efforts to simplify the mesh statements, the specification of the mesh can be a time consuming occupation.

Coordinates in PADLAN must be given in meters or radians. However, this may not be convenient. Therefore the units can be adapted by the unit statements. Per coordinate a unit statement may be given, specifiying a factor by which the given coordinates must be multiplied.

For example, the statement:

$$UNIT(X) = 1.0D-06 \qquad 3.10$$

implies that the x-coordinate can be given in micrometers.

The last statement we want to describe is the symmetry statement. If the structure that is considered has planes of symmetry, the user can impose a symmetrical behaviour of the field at these planes.
Symmetry with respect to a straight boundary surface implies that the B vectors are perpendicular to this surface. Anti-symmetry implies that the B vectors be in the surface.
According to the expected behaviour of the field, the user can apply the symmetry statement. At surfaces where it is not given the program assumes antisymmetry. In this way it is possible to reduce the domain which the problem should be solved in.

3.3. THE PADDY INPUT FOR THE VIDEO HEAD

Before we specified our own mesh, we used an existing one (v.d. Berg, 1981) to gain some experience. With the help of this experience we could formulate some requirements for our own mesh.
They are:
- The mesh definition should be simple and the statements conveniently arranged, so that they can easily be altered and understood by others. As a consequence more statements are used than strictly necessary.
- At the position of the tape the element effect (the normal component of $\underline{B}$ is not continuous when crossing the element's boundary surface, Appendix C) should be restricted to the direction of transportation of the tape (x direction as much as possible).

The second requirement is a consequence of the Fourier Transform, that is carried out on the field along a line of constant z in the x direction at the position of the tape. So z mesh planes should be coordinate planes as much as possible. We have tried to satisfy these demands in the definition of the mesh.

In chapter one we specified the structure of our video head (Figure 1.13). its characteristics are:
- a flat pole-face
- two planes of symmetry (x=0, z=0).

These two assumptions are made to reduce the extent and the complexity of the input of the problem.

Since we are merely interested in the field at the position of the tape and consider the tape in contact with the pole-face everywhere, the assumption of a flat pole-fase is allowed (Figure 3.6).
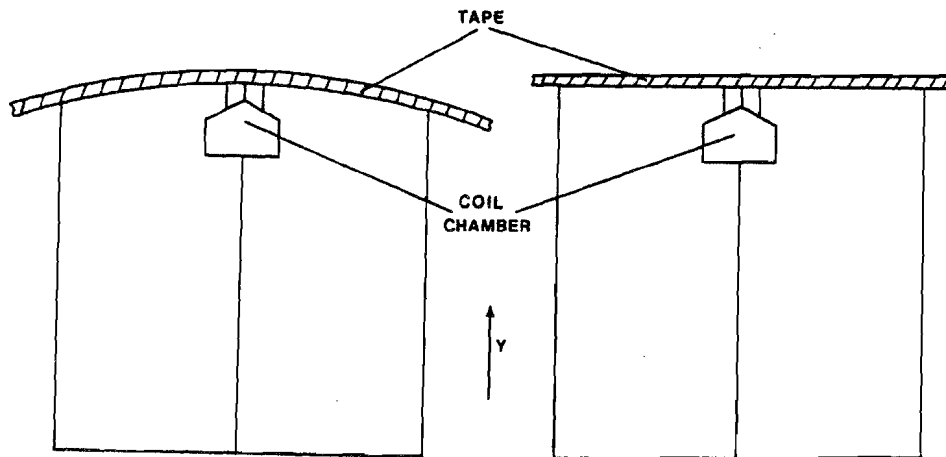
Figure 3.6

Therefore most of the y-mesh planes coincide with the y coordinate planes, which simplifies the input considerably.

The two planes of symmetry offer us the possibility to use the symmetry statement described in the previous section. We expect the flux lines to cross the plane x=o perpendicularly (x=o is an equipotential plane). At the other plane of symmetry, the flux lines lay in the plane (Figure 3.7).
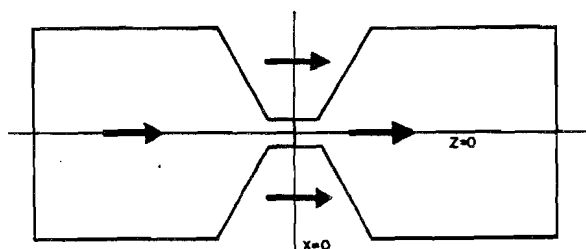
Figure 3.7
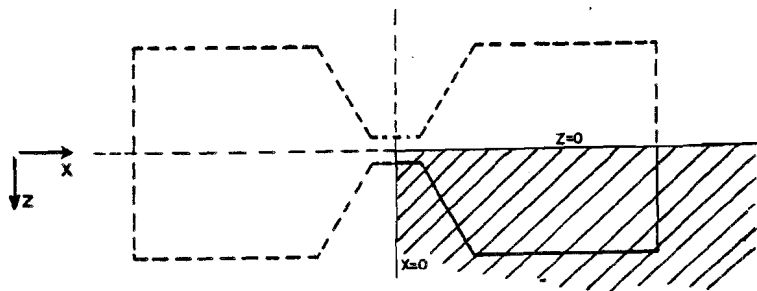
Thus by defining a symmetry statement on x=o (if no symmetry is defined on z=o, the program assumes antisymmetry

we only have to specify a quarter of the videohead and the surrounding air as shown in (Figure 3.7).

For some of the results , the size of the finite part of 3D-space used is important. The dimensions of the finite area are given in fig. 3.8.

The easiest way to define a mesh occurs when <u>all the mesh planes</u> are coordinate planes. All the mesh statements would be of the kind shown in 3.4. This is a situation, which is desirable but cannot be achieved, since at the coil chamber and at the constriction we have sloping sides. Despite these set-backs we will try to describe the mesh on the basis of mesh planes that coincide with coordinate planes as much as possible.
Considering the intersections of the head's material with the x coordinate planes, (Figure 3.8) we see that these intersections contain two quadrangles at most.   .
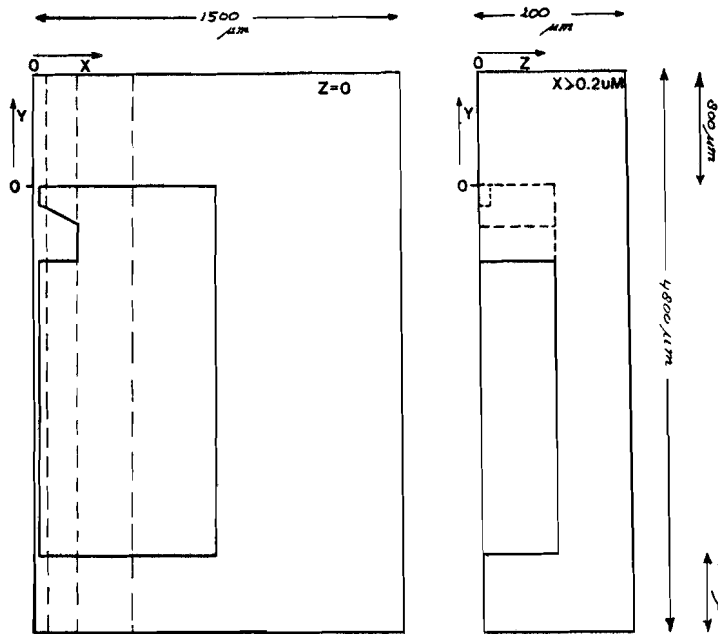
Figure 3.8

Due to the constriction and the structure of the coil changer the upper one of the two quadrangler changes for

$0.2\mu m < x < 400\mu m$. We can distinguish between a change of the upper quadrangle in the positive z direction and a change in the negative y-direction. The former lasts for $20\mu m < x < 108.5\mu m$, the latter for $0.2\mu m < x < 400\mu m$. With the help of Figure 1.13 we can calculate the dimensions of the upper quadrangle for all the x coordinate planes.

If we want to observe our requirement that the y and z mesh planes should be coordinate planes as much as possible, then Figure 3.9 and 3.10 show, how these planes decay as a function of x in the plane of the pole-face and the symmetry plane z=o respectively.
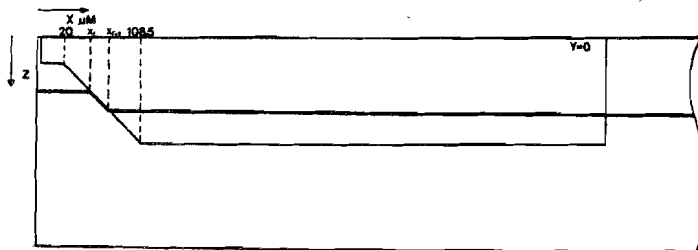
Figure 3.9
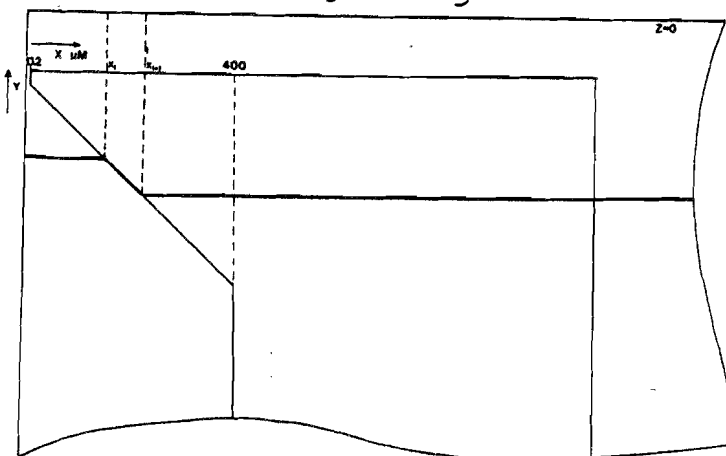
Figure 3.10

It should be noticed, that these planes have to follow the surface of the material for $x_i \leqslant x \leqslant x_{i+1}$ (in these figures.)

By using the possibility of coinciding mesh planes/lines we can obtain the desired behaviour as illustrated in Figure 3.11 for the y mesh plane in Figure 3.11.
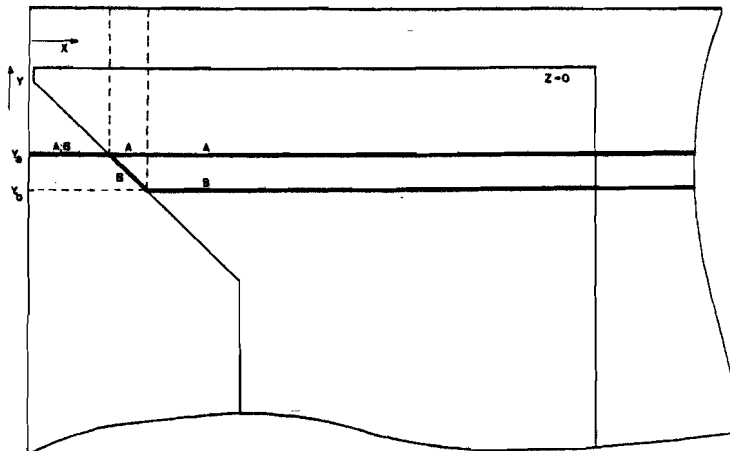
Figure 3.11

For $x \leq x_i$ all x-planes have two coinciding mesh lines A and B with y value Y_A. At plane x_{i+1} mesh line A still has y value Y_A, but meshline B suddenly has Y_B. For $x > x_{i+1}$ this remains the same. PADDY interpolates between the mesh planes and in this way y mesh lines are generated that have the desired behaviour. This can be done in every z-plane and now we have defined a y mesh plane that coincides with the sloping surface of the coil chamber for $x_i < x < x_{i+1}$. The same procedure can be followed at the constriction.

To describe this procedure in mesh statement we have chosen for:
- y as the running variable in the x statements
- z "   "   "   "   " " y "   "
- y "   "   "   "   " " z "   "

In order to arrange the mesh statements in a convenient way, we described the y and z planes in the region 0.2µm < x <   400µm by giving these intersections with the x mesh planes. The statements for the y mesh lines in all these

planes have to result in y mesh planes that, one after an-
other, follow the sloping surface of the coil chamber for a
certain distance in the x direction as shown in Figure 3.12.
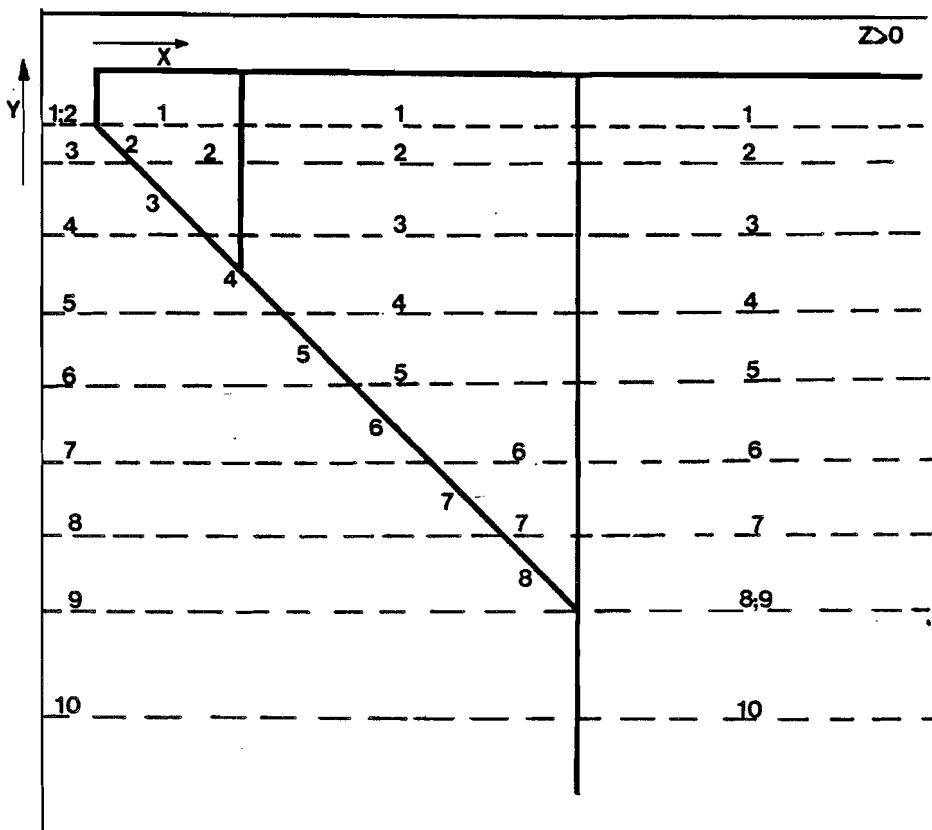
Figure 3.12

The same accounts for the z lines. To make things even
worse, for $20\mu m < x < 108.5\mu m$ the procedure illustrated in
Figure 3.11 should be explored simultaneously for the y and
the z lines. In our case we needed about 700 mesh statements
to describe the mesh of the video head. However per x mesh
plane only minor changes have to be made in the statements
describing the intersecting mesh lines, so most of the work
could be done by the editor of the computer system we used.
Out of the area $20\mu m \leq x \leq 400\mu m$ all planes coincide with
coordinate planes, so we don't pay special attention to the
statements needed.

To reduce the number of unknown at places where the mesh is too refined, compared to the behaviour of the expected field, we can let several mesh planes coincide in all three directions. In our case we restricted the number of unknown to 2.10^4.

In the PADLAN file for our video head we started with the mesh statements. Firstly we specified the y and z lines that are the same for every x plane, because only one statement (as described in section 3.2 statement 3.8 is needed to define such a line in every x plane. After this in <u>each x plane</u> for $0.2\mu m \leqslant x \leqslant 400\mu m$ all the remaining intersecting y and z lines are specified.
For $x > 400\mu m$ the distribution of the intersecting y and z lines does not change anymore. So the statements for these planes are like 3.4 and 3.8 again.

Then the unit statement defines that all the values given in the mesh specification are in micrometers. The symmetry statement is used as discussed previously. For this case Figures 3.13 up and until 3.16 show plots of mesh plane and also the configuration of the head's materials.

The source was chosen identical to the one v.d. Berg (1981) used: a permanent magnet. The strength of this source (the value of the remanent induction: <u>Br</u>) corresponds to the case of an exitation by a coil with 16 turns and a current of 5.325 mA. The μ_z outside the permanent magnet was chosen 500, this is an estimated value (Peters, 1979) for the magnetic permeability of applicated magnetic head materials at the video frequencies (Figure 1.8a). In the permanent magnet of length L=400μm (Figure 3.13), a hard magnetic material, μ is a tensor. The tensor approximately has the form (Zijlstra, 1976):

$$\mu_z(\underline{H}) = \begin{pmatrix} \mu_z(H_{//}) & 0 \\ 0 & \mu_{z\perp} \end{pmatrix} \qquad\qquad 3.9$$

$H_{//}$ is the component in the direction of $\underline{B}r$. In our case $\underline{B}r$ = $-Br$ $\underline{i}_Y$ and $\mu_{//}$ = 500 for $\mu_{//}$ also the value 500 is chosen. This is done to simulate the situation in the soft magnetic material as much as possible.

The problem can only be solved in a restricted domain, shown in Figures 3.13 and 3.14. The boundaries of the mesh may not be too close to the boundaries of the head, to avoid influence on the field near the head. On the other hand, they should not be too far away, in order to restrict the number of unknowns. This, again implies a compromise.

By means of a TEST statement in the input file, plots of mesh planes can be made like those in Figures 3.13 up and including 3.16. This offers a possibility to check if the mesh statements represent the desired pattern.

At the gap the mesh is more refined, since we expect a strongly varying field there. In Figures 3.15 and 3.16 the areas of the coil chamber and the constriction are enlarged. It can be seen now, how the y and the x planes decay as a function of x at the sloping sides of the heads material. Also the coinciding planes to reduce the number of unknown can be noticed.
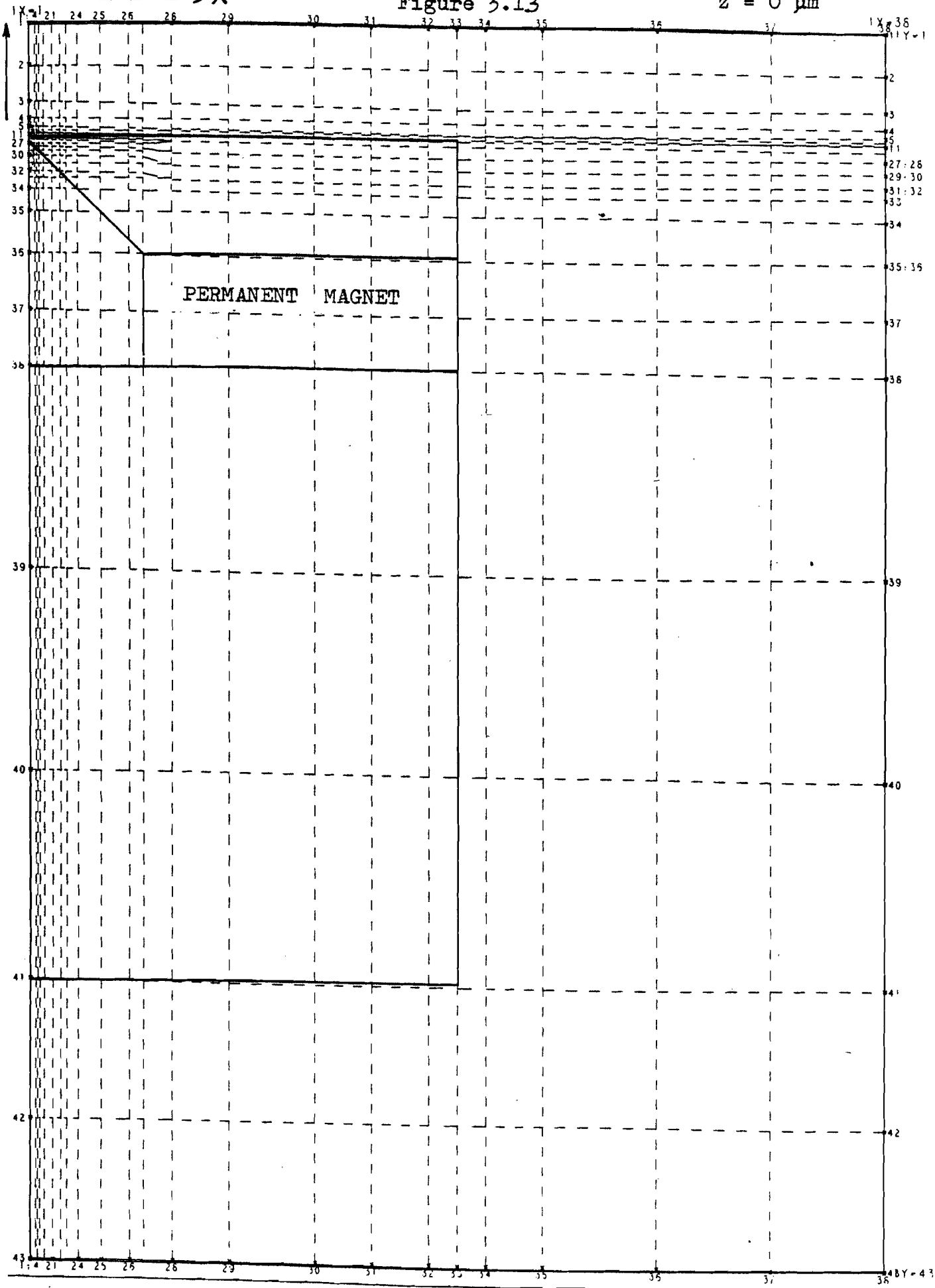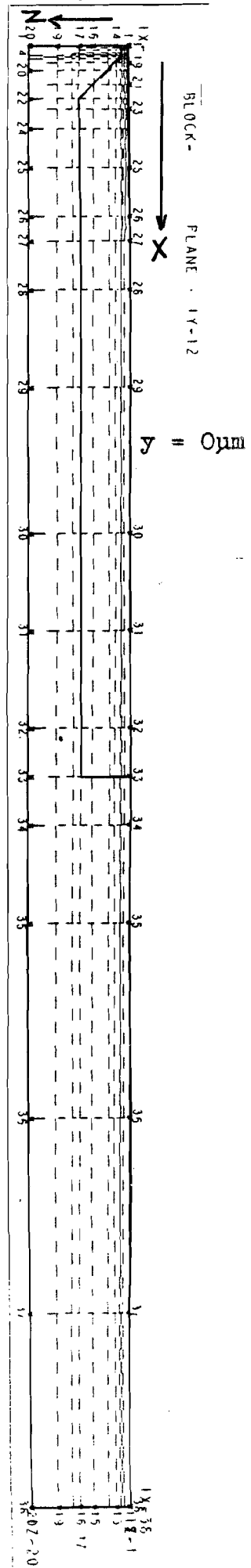
BLOCK-   PLANE · IZ-1

Figure 3.13

z = 0 μm

PERMANENT MAGNET

Figure 3.14

5895

BLOCK-

PLANE · IY·12

y = 0µm

Figure 3.15   z = 0 um

Figure 3.16   y = 0 µm

PHILIPS

CHAPTER FOUR

RESULTS OBTAINED WITH PADDY

4.0 INTRODUCTION

4.1 RESULTS OBTAINED WITH THE VIDEO MESH

4.2 RESULTS OBTAINED WITH A REFINED MESH

4.3 COMPARISON OF RESULTS

4.0 INTRODUCTION

In chapter 4 the results obtained with PADDY are pre-
sented and discussed. Firstly the results of the video mesh
as described in Chapter 3 are given. Then a refined part of
this mesh is defined and a potential is imposed on its boun-
daries, the results of this calculation are shown in Section
4.2. Finally a comparison is made between the PADDY results
and the results of the video head model of section 2.2.

4.1. RESULTS OBTAINED WITH THE VIDEO MESH

After the problem is defined (Section 3.3) the PADDY
job can be started. The results are presented in plots
and/or prints of the different quantities. It can be checked
now, if the output satisfies the following physical expecta-
tions.
- The decay of the potential can give information about the
  quality of the mesh. A carefully chosen mesh will show no
  non physical changes in the sign and the value of the
  field components.
- The value and the homogeneity of the field in the gap.
- The value of the z component in the symmetry plane (z=o).
- The boundary conditions at the surface of the medium.
In 4.3. a comparison with the results of our video head mo-
del will be made.

The gap field is almost homogeneous:
$\underline{H}=H_x \underline{\hat{x}}$ and $H_x \approx 1.4.10^5$A/m. With this value the so-called
efficiency η of the head can be calculated.

$$\eta = \frac{\int\limits_{GAP} \underline{H}.\,d\ell}{\oint\limits_{HEAD} \underline{H}.\,d\ell} = \frac{\int\limits_{GAP} \underline{H}.\,d\ell}{NI} \qquad\qquad 4.1$$

The efficiency is in fact the relation betweent he potential
jump over the gap devided by the M.M.F. of th source.
was found to be : 66%, in agreement with Vd Berg (1981).

The values of the Hz component of the magnetic field in
z=0, were almost zero as expected. So in z=p the magnetic
field lines can be imagined as the orthogonal trajectories of
the equipotential lines. In Figure 4.1 a plot of these lines
is given in z=o.
The lines denote a constant increment of the value of
the potential. We see that this value increases   linear
in the permanent magnet. The larger distance in the soft
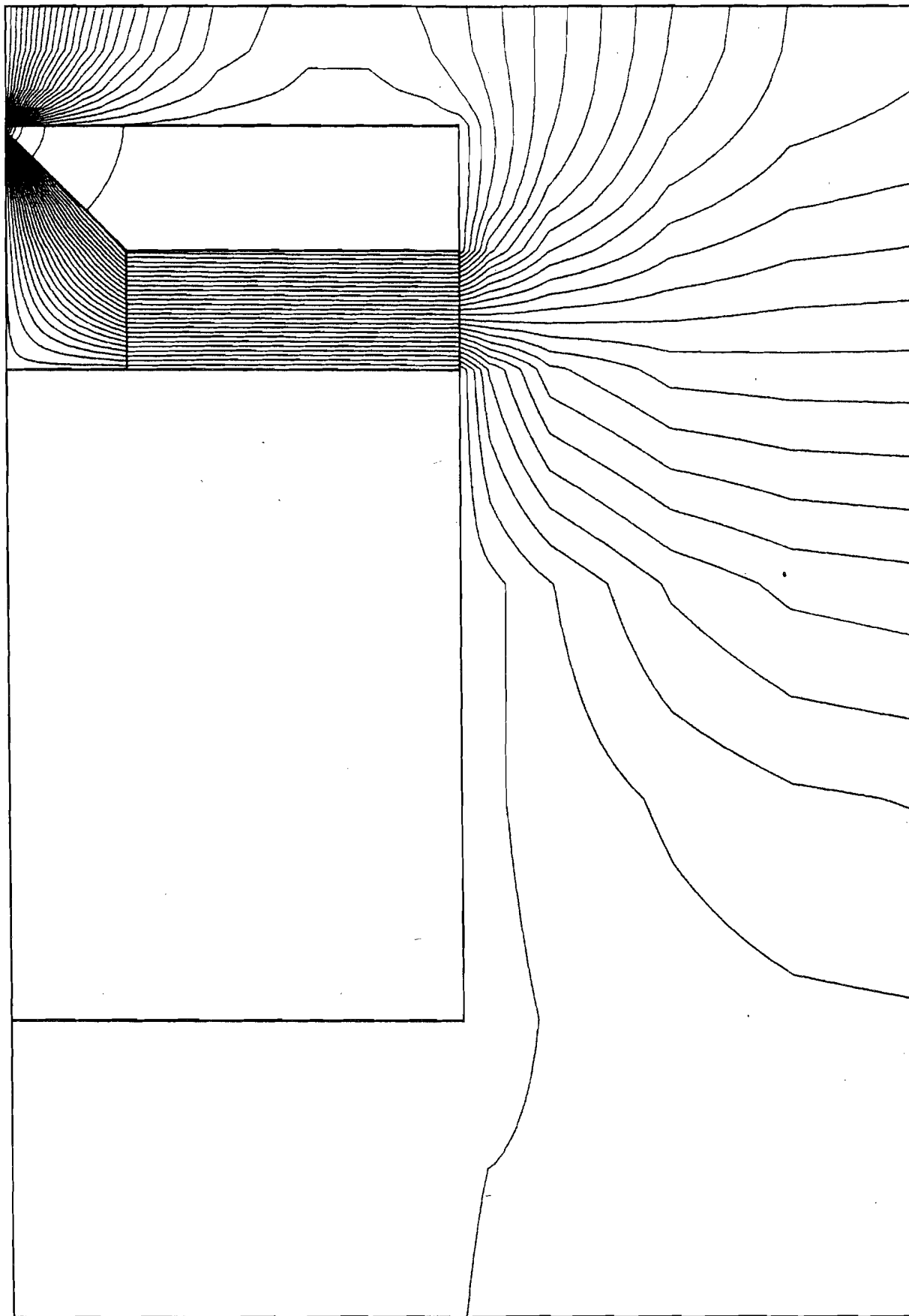
Figure 4.1

z = 0 um

PHILIPS

magnetic material compared to the air, is due to the difference in μ . Outside the head and in the coil changer the flux leakage can be seen.

Due to the relatively high value of μ_R in the soft magnetic material, the field lines are almost perpendicular to the surface. In Figure 4.2 the equipotential lines near the gap are shown
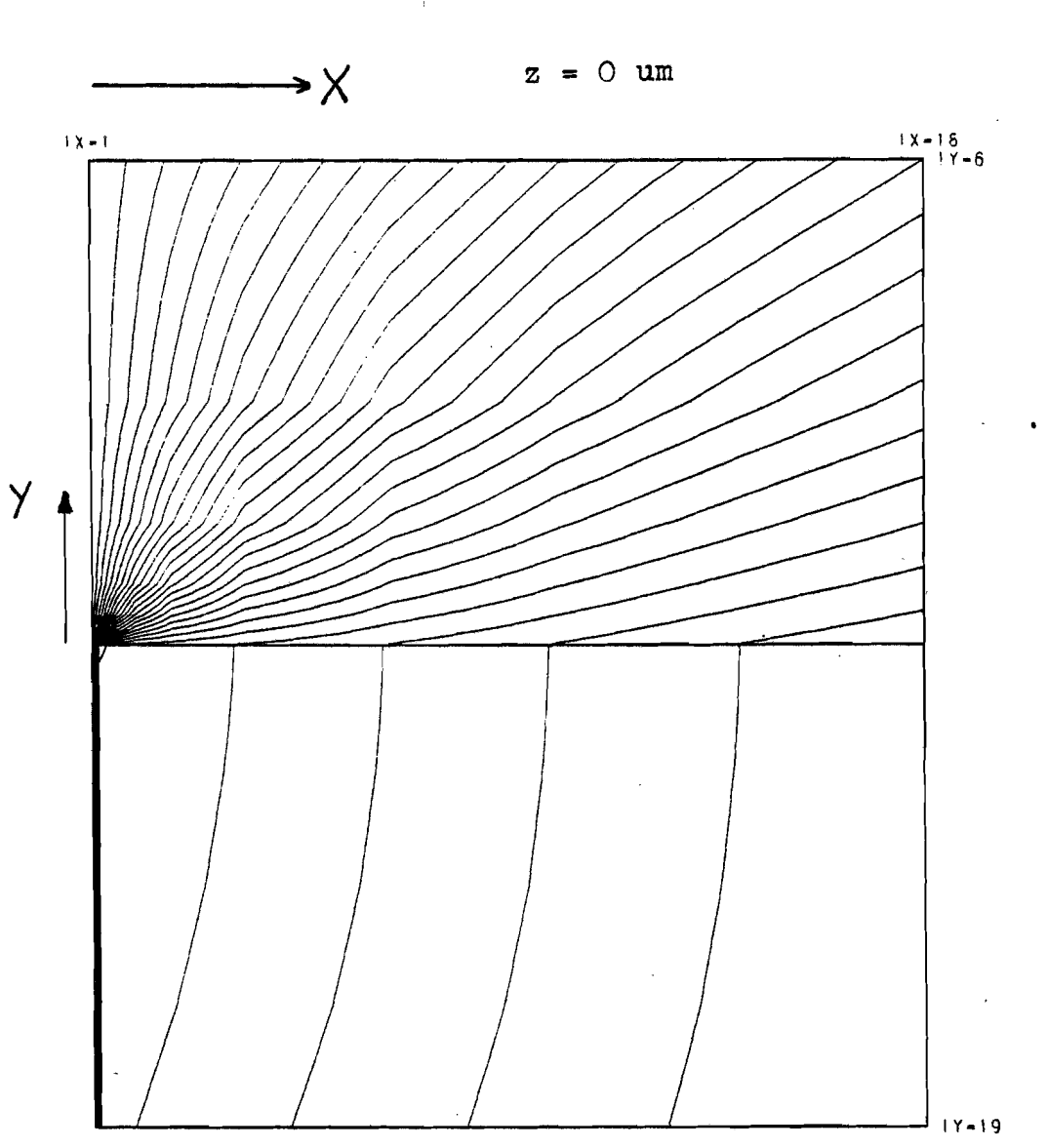
Figure 4.2

After verification of the results, another characteristic of the head can be calculated: the self inductance L . Together with the resistance and the stray capacity of the coil, the self inductance of the head forms a resonance circuit.

In a recording system (e.g. videorecorder) one has to avoid a strong resonance in the frequency range of interest. On the other hand it is advisable to use as many turns as possible, to enhance the read signal. This implies a compromise. For the calculation of the self inductance.

$$L = \left(N \iint_{\substack{CROSS- \\ SECTION \\ HEAD}} B \cdot dA \right) / I \quad (HENRY)$$

4.2

we need the flux in the head, cause by the source:

$$\Phi = \iint B \cdot dA \quad (WEBER)$$

4.3

Φ is calculated in the permanent magnet at y=700µm. In this calculation a factor 2 should be included accounting for the fact that only a quarter of the head was implemented (Figure 3.8). Furthermore one should bare in mind that the total head is excited by two permanent MAGNETS of equal strength and opposite sign. Figure 4.3.

700 um
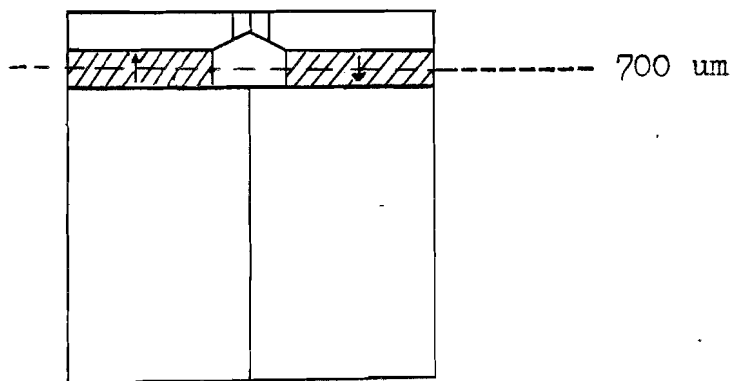
Figure 4.3

The self induction is found to be

$$L \approx 0.85 \, \mu H$$

Measurements on practical video heads give a self induction of   1.5µH. The difference can be due to the fact that:
- a permanent magnet is used instead of a coil
- μ_r is assume to be a constant
- the structure of our video head is an approximation of a real video head.
- It appears that a large fraction of the flux does not reach the gap. It leaks away outside the soft magnetic circuit. This leakage flux does contribute to the inductance. The amount of leakage flux is probably rather low in this problem because of the rather small $part$ of 3D-space, that is taken into account in the z-direction (and positive y-direction). As a concequence the self inductance may be under estimated.

We now proceed with the magnetic field strength along lines of constant z value in a plane at the position of the tape. A post processing routine (Section 3.1) was used to obtain the values of the field componets. The H_x -and the Hy component are shown in Figure 4.4 and 4.5. PADDY calculates only in a quarter part of the total area (Figure 3.8). Therefore the results are extended to the total area (with the proper sign) by using the already symmetry properties of the head (page 19).

    The results are normalised on the deep gap field. The pole-face of the videa head is shown too.

5895
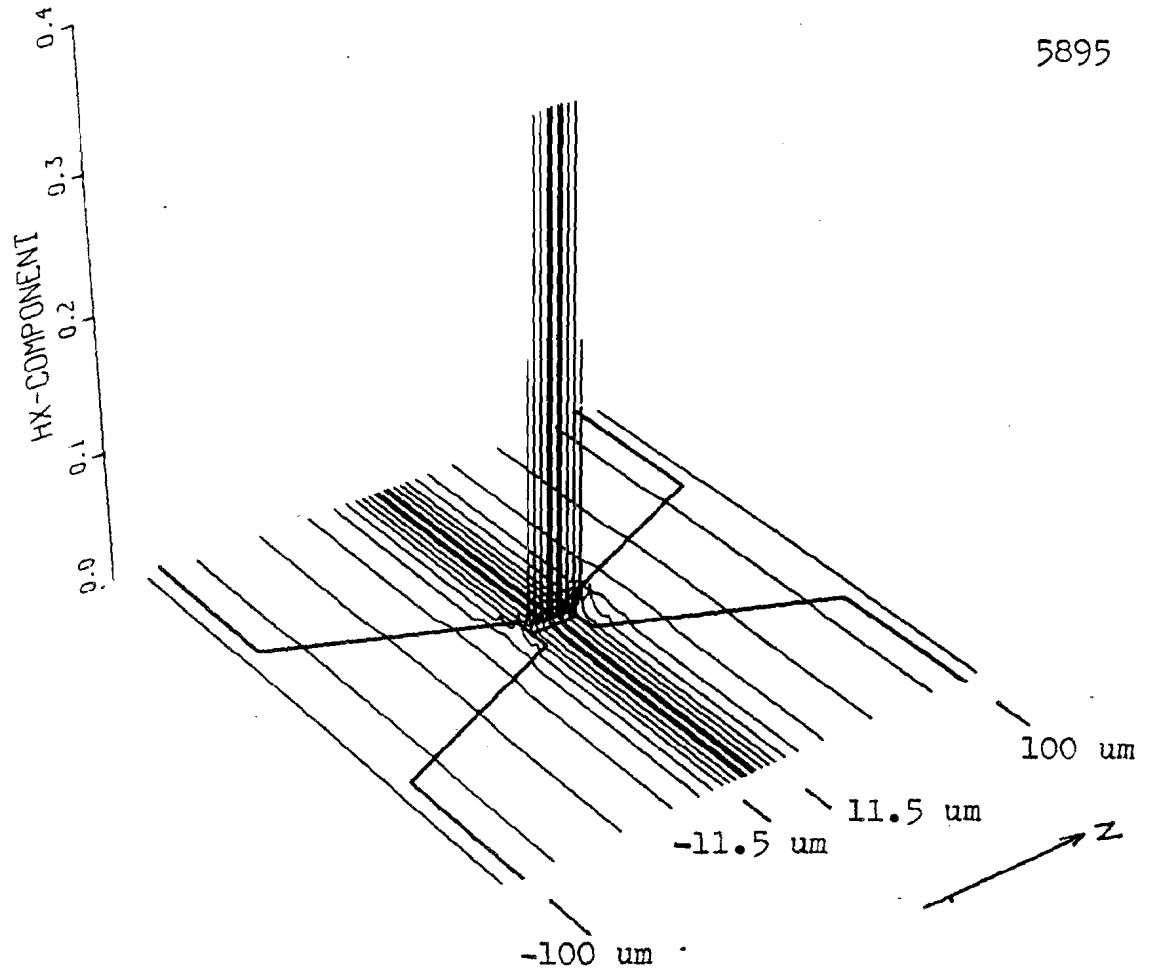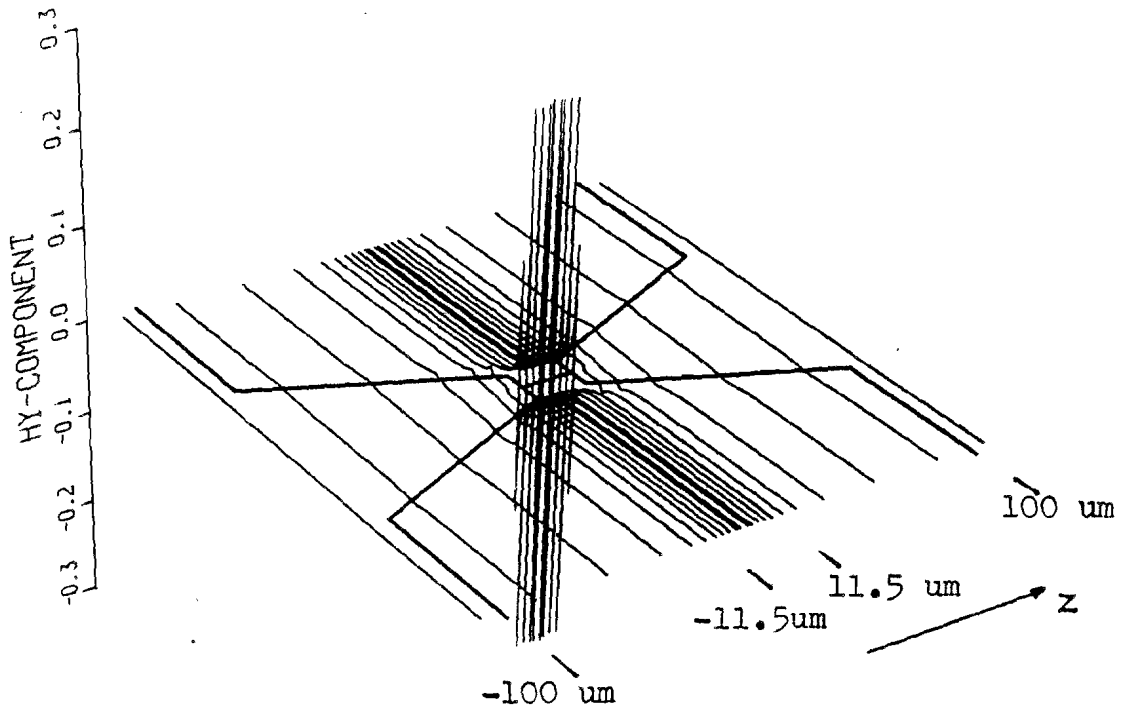
Figure 4.4

Figure 4.5

We notice that the H_x component reaches its maximum exactly above the gap. The value of the maximum decreases quickly for increasing $|z|$. Hy shows the expected asymmetrical behaviour. The Hz component differs significantly from zero only at the edge of the gap and is omitted here.

For z values near the edge of the gap we see the influence of both the gap and the constriction. In Section 4.2, with the help of a more refined mesh, more detailed plots of the magnetic field components at the constriction are given.

4.2. RESULTS OBTAINED WITH A REFINED MESH

Despite the fact that there are almost 2.10^4 nodes, the number of nodes along a line of constant z value for (Figure 3.8) is only 38.
In order to describe the effect of the construction properly this number should be increased.

In PADDY there is a possibility to refine the mesh in a certain area and impose a potential on the new boundaries. The boundary potential should be calculated form the results of the original problem of the video head. This is done for the area shown in Figure 4.6 and 4.7.
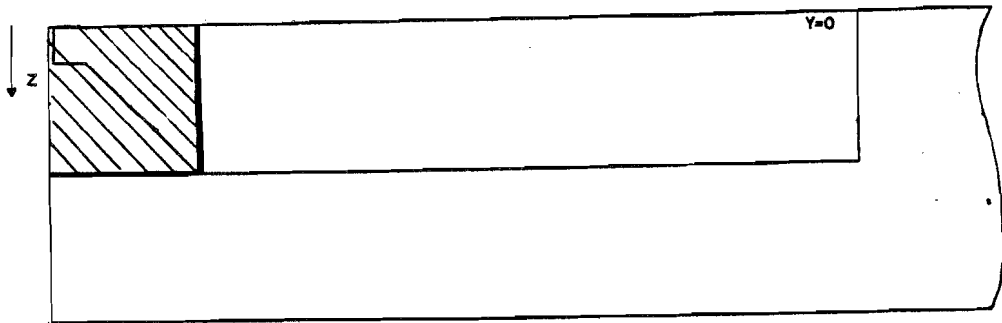
Figure 4.6
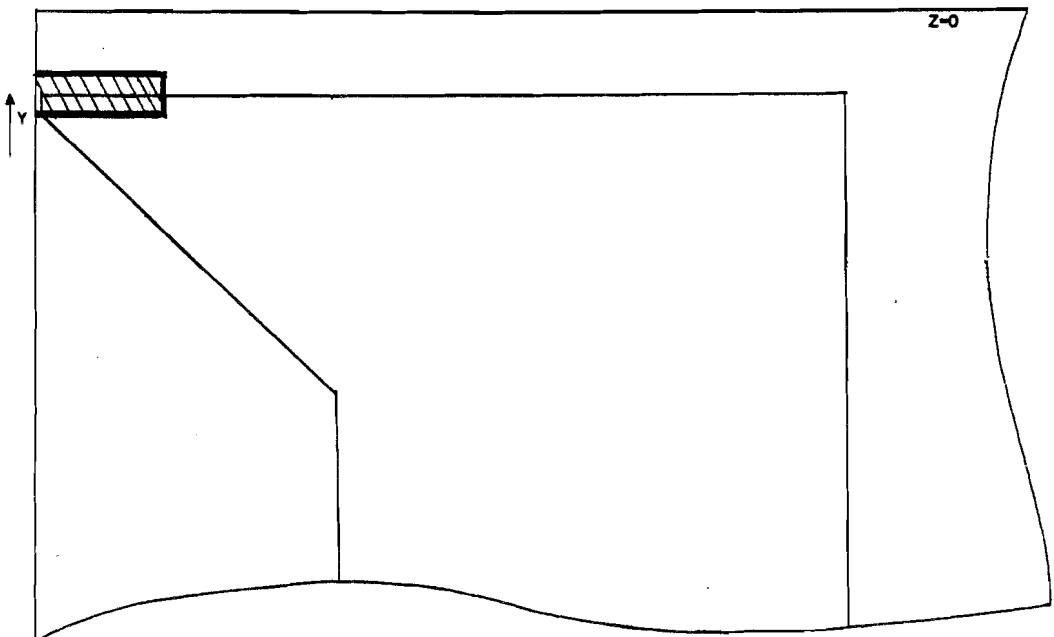
Figure 4.7

The potential at the boundaries is calculated by means of the following procedure.

1. Define a <u>new PADDY problem</u> (in a restricted domain of the original problem) with a mesh, material specification etc. and a FORTRAN function (section 3.1): FPOT. This function gives the potential in the nodes at the boundaries of the new mesh. PADDY calculates all the nodes in the mesh and asks for the potential in the nodes at the boundary. Since this potential is unknown yet, FPOT is made zero, meanwhile the coordinates of these nodes are stored in a file.

2. The file with the coordinates serves as an input file for a post processing job (Section 3.1) on the results of <u>the original problem</u>. In these boundary nodes the post-processing job asks for the potential. The new mesh is more refined than the original one, so interpolation of the original results is necessary. PADDY takes care of that (Appendix C). In this way a new file can be made, with the coordinates and the potential at the boundary nodes.

3. The new PADDY job is runned with this file as an input file.

PHILIPS

The new mesh is generated in the same way as the origi-
nal one (Section 3.3), with the difference that there is on-
ly one sloping side now: the one of the constriction. The
new mesh is illustrated in Figure 4.8 and 4.9.

BLOCK-   PLANE : iy=11

⟶ X   y = 0 um
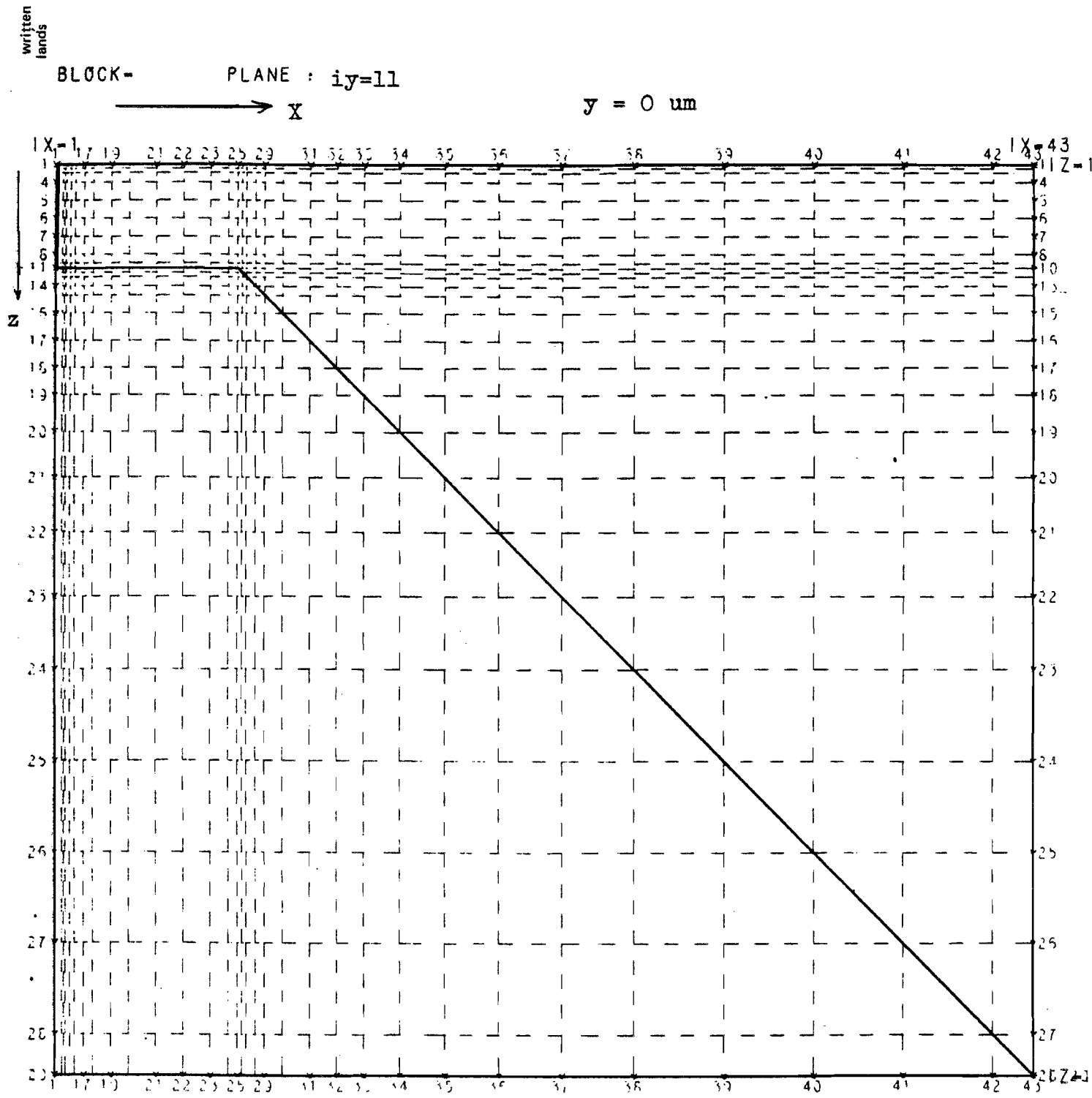
Figure 4.8

z = 0 um
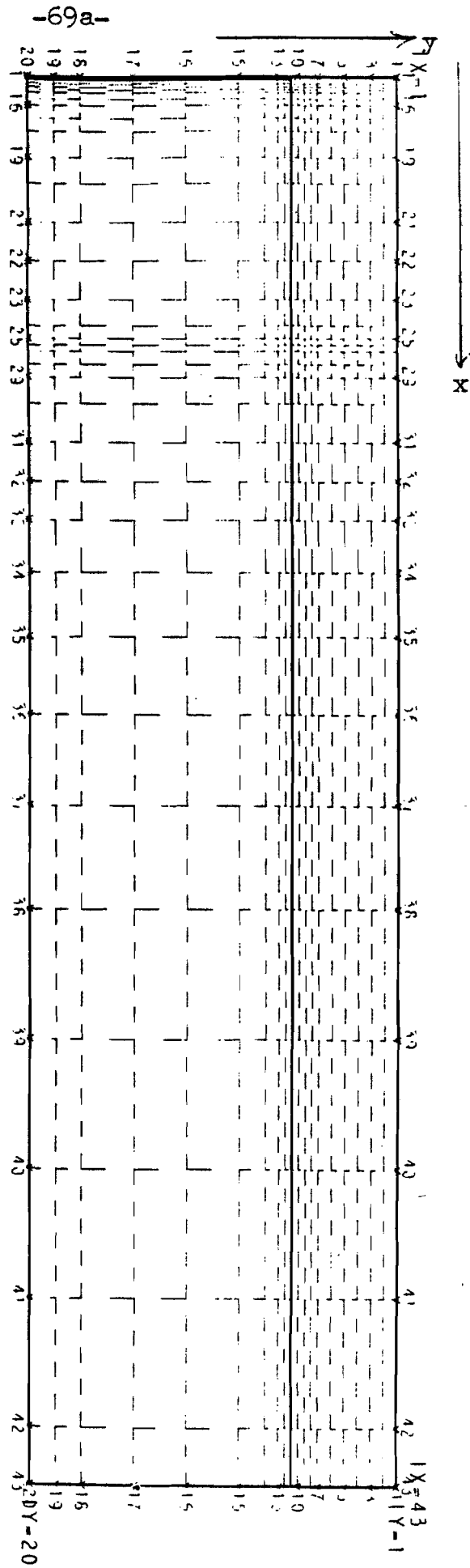
Figure 4.9

The results obtained with this mesh are shown in Figures 4.10 and 4.11.

In these Figures we notice:

- The decay of the H_x and Hy as already seen in Figures 4.4 and 4.5. The maximum of the H_x is twice the value of the extrema of Hy. The same phenomenon can be found in the Karlquist model (De Hoop, 1976).

- At z=12.0μm the influence of the constriction is hardly perpceptible, while the gap fringing has decreased only with a factor 2.

- At z=20.0μm there is still the influence of the gap, but the contribution of the constriction has increased.

- At z=40.0μm there is only the effect of the constriction left. Compared to the results at z=20.0μm the extreme have smaller values.
- Due to the boundary condition at the pole face, the component is almost zero above the material. The extreme in Hy are reached after crossing the sloping sides of the construction.

- Even in this refined mesh a lack of "field points"(nodes) is displayed at the constriction.
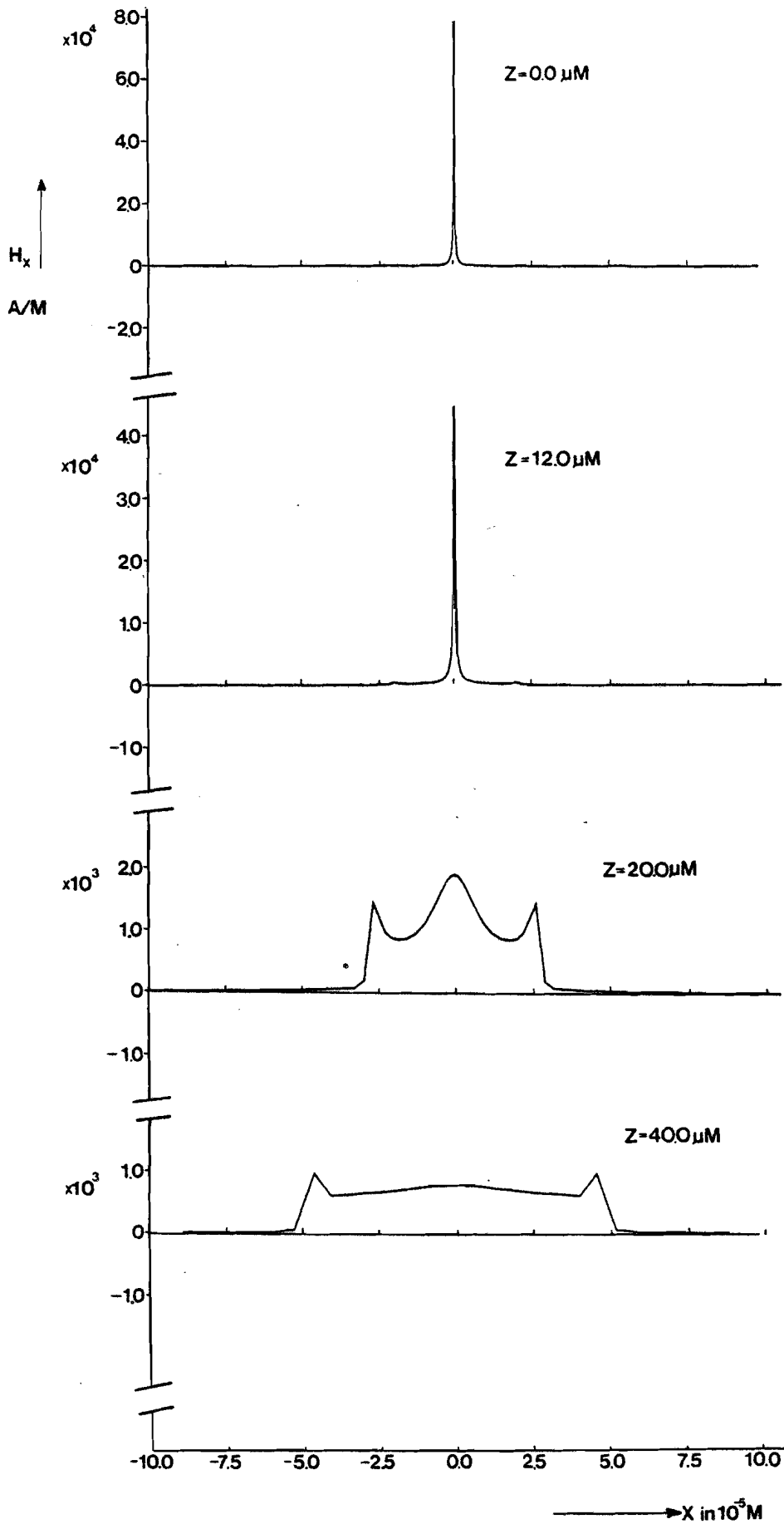
Figure 4.10

H_y COMPONENT OF VIDEO HEAD
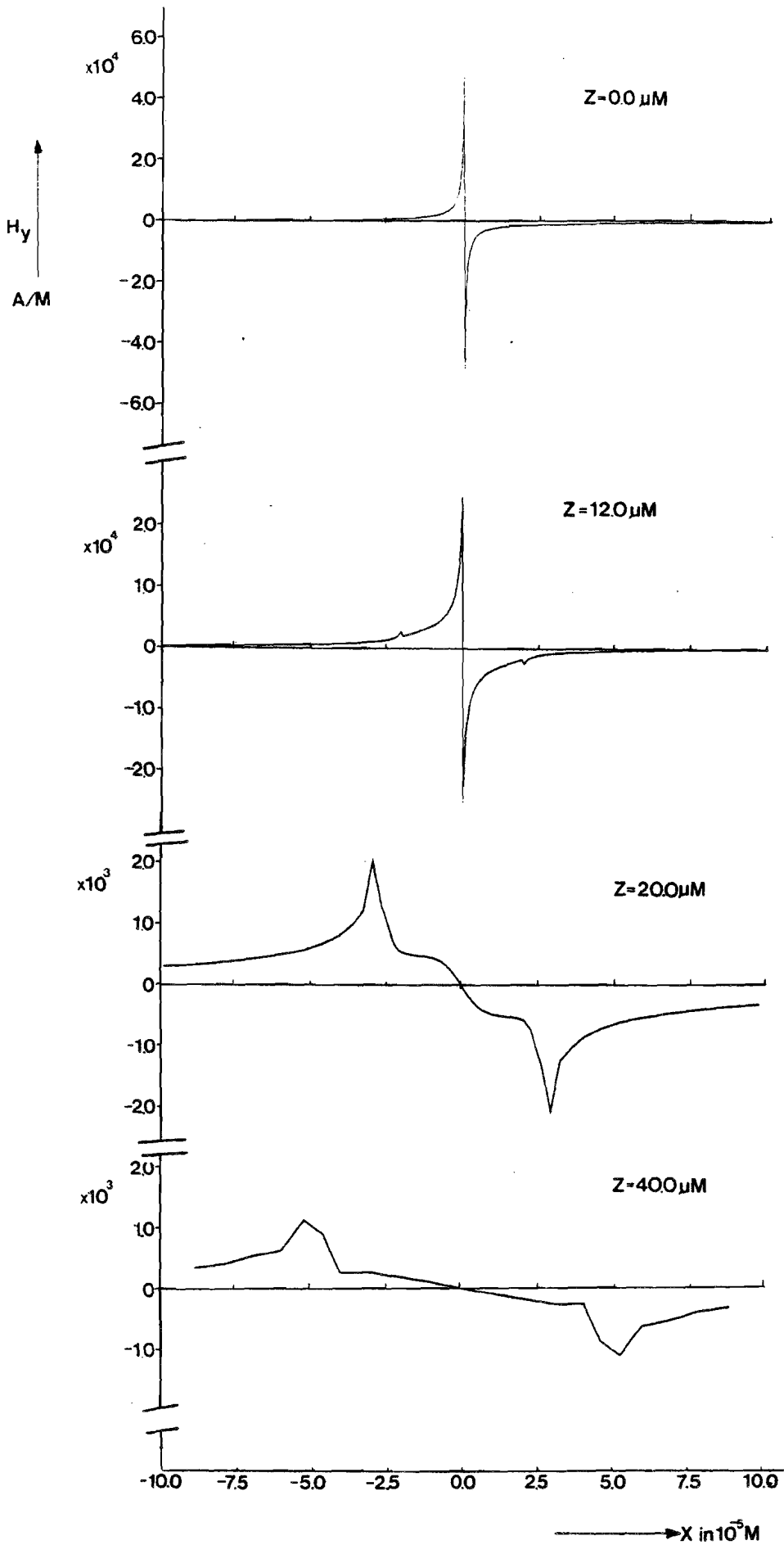
Figure
4.11

If the results of the original and the refined problem are combined, the number of field points is raised from 38 to 58 for $x \gtrless 0$ (The Fourier Transform in Chapter was calculated with about 400 field points in the range $x \gg 0$). Furthermore since.

$$\int_{-\infty}^{\infty} H_{x,y}\, e^{jkx}\, dx \bigg|_{k=0} = \int_{-\infty}^{\infty} H_{x,y}\, dx = 0$$

the sensitivity functions should decrease for large wavelengths ($\lambda \rightarrow \infty$, $k \downarrow 0$). In PADDY the potential is calculated in a finite domain. Therefore the Fourier Transform of the PADDY results for wavelengths of about the length of the domain (in the x direction, and larger) will be unreliable.

The numerical F.T. of the PADDY results is further complicated by the lack of field points. In Figure 4.12 only the results of $|\tilde{H}_x(k;y,z)|$ are shown for z=0.0 and z=12.0μm.

In Figure 4.12 we see that the first dip is at the right wavelength for z=o. At z=12.0μm the sensitivity function has lower values, but the same form as the one at z=o. This shows that the effect of the construction is only minor compared to the effect of the gap at this line. For higher z values the first dips are at the expected wavelengths (not shown here).

In conclusion we can remark that the effect of the constriction is shown along z lines not too close to the edge of the gap. So suppression of video frequencies due to the constriction works well, except for the adjacent tracks.

SENSITIVITY   FUNCTIONS   VIDEO HEAD   IN Y=0.25μM
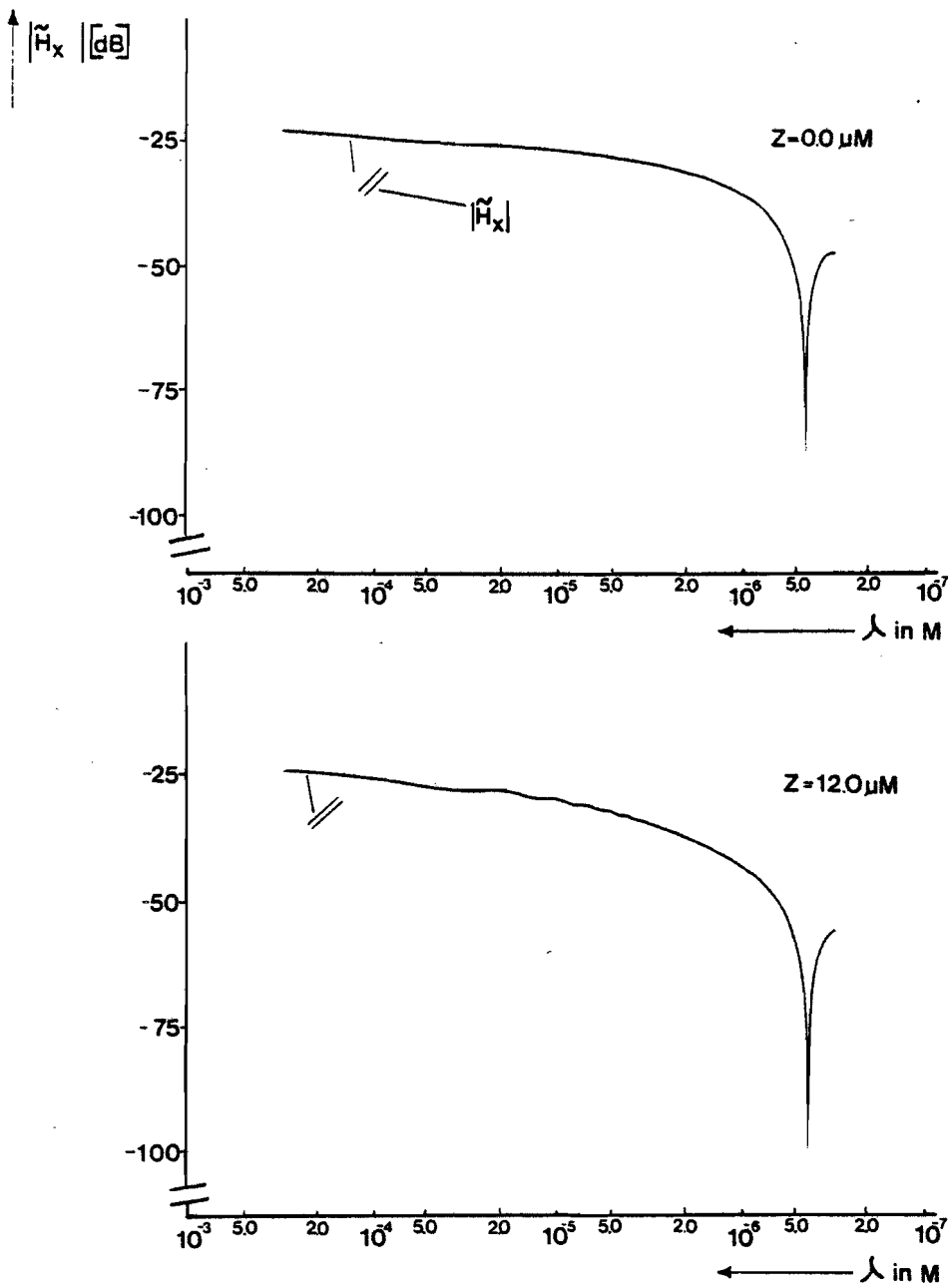
Figure 4.12

4.3. COMPARISON OF RESULTS

In this section we compare the results obtained with the video head model (briefly called: "model" here) of Section 2.2 and the PADDY results (called the results of: "the video head".

The following remarks can be made:

- Near the gap the field of the video head is larger than the field of the model, despite the fact that both of them have the same homogeneous gap field.

- The extrema in H_x and Hy of the video head along lines of constant z value above the constriction, decrease for increasing $|z|$ values. This is due to the increasing distance of the sloping sides. Since the surface density of the sloping plates in the model is a constant, this decrease is not shown in the video head model.

- As a consequence of the first remark, the influence of the constriction near the edge of the gap is hardly perceptible in the magnetic field of the video head, in contrast to the model.

- The Fourier Transform of the magnetic field along lines of constant z at the plane of the tape shows the secondary gap effect clearly. The F.T. of the corresponding PADDY results is reliable only for small wavelengths and small $|z|$ values.

Considering these remarks it can be noticed, that there is quite a difference between the video head and the model. This is due to the absence of the proper boundary conditions, caused by the magnetic material of the head. However as already stated in section 2.2, the video head model is only used to describe the effect of the constriction. It was not our purpose to approximate the field of a video head

with this model.

However, it should be noted here that in principle the field of the video head can be approximated analytically by taking into account <u>all</u> the charged planes at the surface of the video mesh and by deriving the surface charge from PADDY.

PHILIPS

8222 256 95021

PHILIPS

FINAL CONCLUSIONS AND FOLLOW UP

At the end of this report we give some final conclu-
sions and some possibilities for a continuation.

Although the PADDY calculation results in a reliable
field in the head and in the area next to it, it is diffi-
cult to study the crosstalk of neighbouring tracks by means
of the Fourier Transform of the magnetic field along lines
of constant z value at the place of the tape.

To improve the results of the numerical Fourier Trans-
form, smoothing of the PADDY results is necessary. Further-
more the field at larger distances should be approximated by
an analytical function.

A first step towards another way of smoothing the PADDY
results is given in Chapter 2. In this Chapter an expression
is derived for the magnetic field strength of a plane homo-
geneously charged quadrangle. The surface of the video head
as specified in the mesh, consists of quadrangles and
triangles, that can be thought to have a constant surface
charge density:

$$\nabla_M(\underline{r}') = (\underline{M}(\underline{r}') \cdot \underline{n}) \qquad 5.1$$

It is possible now, to calculate the magnetic field in
every point in principal, by summation of all the contribu-
tions of the charged polygons on the surface of the head.
The implementation of this calculation on a computer is a
time consuming affaire, for which there was no time left in
this graduation period. Instead, the simple models of Chap-
ter 2 were implemented. The results of these models, look
very promising.

mk/kvk   Eindhoven, November 1983
                                Philips Research Laboratories
                                Nederlandse Philips Bedrijven B.V.

8222 256 95021

LIST OF REFERENCES

1) Bahr, H. (1981)
   Alles über Video
   Philips Taschenbücher T21

2) Chi, C.S. (1974)
   A dynamic iterative model for digital magnetic recording
   Thesis, Worcester Polytechnic Institute
   USA

3) De Beer A., Polak S., Wachters A. and van Welij, J.,
   (1981)
   PADDY user manual
   TIS-CARD/Mathematical Software Group
   Philips Nederland B.V.

4) De Hoop, A.T. (1977)
   Topics in magnetic recording
   Lecture Notes, Delft University of Technology
   The Netherlands

5) Iwasaki, S. and Nakamura, Y. (1977)
   An analysis for the magnetization mode for high density
   magnetic recording
   IEEE Tr. on Magn., MAG-13 (10), 1272-1277

6) Karlqvist (De Hoop, 1977)

7) Luitjens, S. and Van Herk, A. (1982)
   A discussion on the crosstalk in longitudinal and
   perpendicular recording
   IEEE Tr. on Magn. Vol. MAG-18 (6)

8) McCary, R.V. (1971)
   Saturation magnetic recording process
   IEEE Tr. on Magn. Vol. MAG-7 (1), 4-16

9) Peters, C.A.J. (1979)
   The calculation of the electromagnetic fields of the
   video head V2000 with the help of the program package
   MAGGY 2
   Report of the practical work (THE)
   Philips Nederland B.V.

10) Strang, G. and Fix, G. (1973)
   An analysis of the finite element method
   Prentice-Hall Inc.

11) Van Den Berg, A. (1981)
   The magnetic field of a video head calculated with the
   program package PADDY
   Report of the practical work (THE)
   Product Division Video
   Philips Nederland B.V.

12) Van Herk, A. (1977)
   Side fringing field and write and read crosstalk of
   narrow magnetic recording heads
   IEEE Tr. on Magn. Vol. MAG-13, 1021-1028

13) Van Herk, A. (1980)
   Three-dimensional analysis of magnetic fields in
   recording head-configurations
   Thesis, Delft University of Technology
   The Netherlands

14) Westmijze (1953)
   Studies on magnetic recording
   Philips Research Reports Vol. 8
   May, June, August and October

APPENDIX A

THE MAGNETIC-FIELD STRENGTH OF A PLANE HOMOGENEOUSLY CHARGED QUADRANGLE

The expression for this magnetic field is given by 2.12

$$\underline{H}_A(\underline{r}) = \tau_M \iint\limits_{A(\underline{r}')} \nabla' G(\underline{r}, \underline{r}') \, dA(\underline{r}') \qquad\qquad 2.12$$

First we designate

$$R = |\underline{r}' - \underline{r}| = \left[(\underline{r} - \underline{r}') \cdot (\underline{r} - \underline{r}')\right]^{1/2} \geqslant 0 \qquad\qquad A.1$$

and rewrite:

$$\underline{H}_A(\underline{r}) = \frac{\tau_M}{4\pi} \iint\limits_{A(\underline{r}')} \underline{\nabla}' R^{-1} \, dA(\underline{r}') \qquad\qquad A.2$$

$$\underline{\nabla}' R^{-1} = (\underline{n}_Q \cdot \underline{n}_Q) \underline{\nabla}' R^{-1}$$

$$\underline{n}_Q \times (\underline{\nabla}' R^{-1} \times \underline{n}_Q) + (\underline{n}_Q \cdot \underline{\nabla}' R^{-1}) \underline{n}_Q =$$

$$(\underline{n}_Q \times \underline{\nabla}' R^{-1}) \times \underline{n}_Q + (\underline{n}_Q \cdot \underline{\nabla}' R^{-1}) \underline{n}_Q =$$

$$(\underline{n}_Q \times \underline{\nabla}' R^{-1}) \times \underline{n}_Q R^{-1} + (\underline{n}_Q \underline{\nabla}' R^{-1}) \underline{n}_Q \qquad A.3$$

A.3 is a decomposition of $\underline{\nabla}' R^{-1}$ in a component perpendicular to $\underline{n}_Q$ and one parallel to it. $\underline{n}_Q$ is a constant vector on A.

$$\underline{H}_A(\underline{r}) = \frac{V_M}{4\pi}\iint\left((\underline{n}_Q \times \underline{\nabla}') \times \underline{n}_Q \, \mathcal{R}^{-1} + (\underline{n}_Q \cdot \underline{\nabla}'\mathcal{R}^{-1})\underline{n}_Q\right) dA(\underline{r}') \qquad A.4$$

On account of Stokes' theorem we have (Figure A.1):

Figure A.1

$$\iint_{A(\underline{r}')}(\underline{n} \times \underline{\nabla}') \times \underline{n}_Q \, \mathcal{R}^{-1} dA(\underline{r}') = \oint_{C(\underline{r}')}(\underline{\tau} \times \underline{n}_Q)\mathcal{R}^{-1} dC(\underline{r}')$$
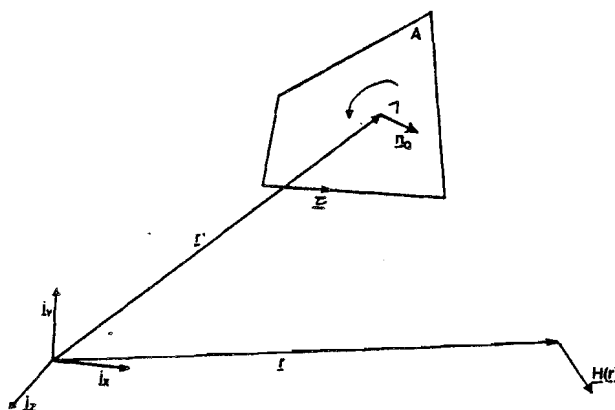
$$= -\underline{n}_Q \times \oint_{C(\underline{r}')} \underline{\tau} \, \mathcal{R}^{-1} dS(\underline{r}') \qquad A.5$$

C denotes the boundary contour of the quadrangle A and $\underline{\tau}$ is the unit vector along the tangent to C in the direction of circulation along C, the latter forming a right-handed system with $\underline{n}$.

Now we can write for A.4

$$\underline{H}_A(\underline{r}) = \frac{V_M}{4\pi}\left[-\underline{n}_Q \times \oint_{C(\underline{r}')} \underline{\tau} \, \mathcal{R}^{-1} dC(\underline{r}') + \underline{n}_Q \iint_{A(\underline{r}')}(\underline{n}_Q \cdot \underline{\nabla}'\mathcal{R}^{-1})\underline{n} \, dA(\underline{r}')\right] \qquad A.6$$

The second integral in A.5 is the signed solid angle   at which A is observed from the point of observation

$$\iint_{A(\underline{x}')} \underline{n}_\varphi \cdot \underline{\nabla}' R^{-1} \underline{n}_\varphi \, dA(\underline{x}') = \frac{\underline{n}_\varphi \cdot (\underline{x}'-\underline{x})}{|\underline{n}_\varphi \cdot (\underline{x}'-\underline{x})|} \iint_{A(\underline{x}')} \frac{\underline{n}_\varphi \cdot (\underline{x}'-\underline{x})}{|\underline{x}'-\underline{x}|} dA(\underline{x}')$$

$$= -sgn\left(\underline{n}_\varphi \cdot (\underline{x}'-\underline{x})\right)\omega = \Omega \qquad\qquad A.7$$

So Ω is negative when the point of observation is at the same side of the quadrangle as to where $\underline{n}_\varphi$ points (a in Figure A.2) and is positive in the other case (b).
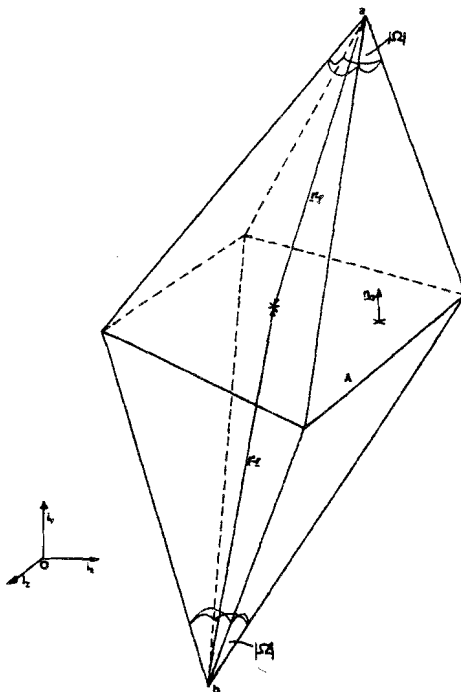
Figure A.2

For the solid angle Ω an expression in terms of geometrical quantities can be derived. To obtain this expression we

project the quadrangle on a sphere of unit radius and centre at the point of observation. The numerical value of Ω is then equal to the area of the resulting spherical quadrangle. We can express this area in terms of the angles (α m) that are included by the planes that pass through the sides of the spherical quadrangle (and hence through the sides of the quadrangular disk) and the centre of the sphere.

sphere of
unit radius

point of observation
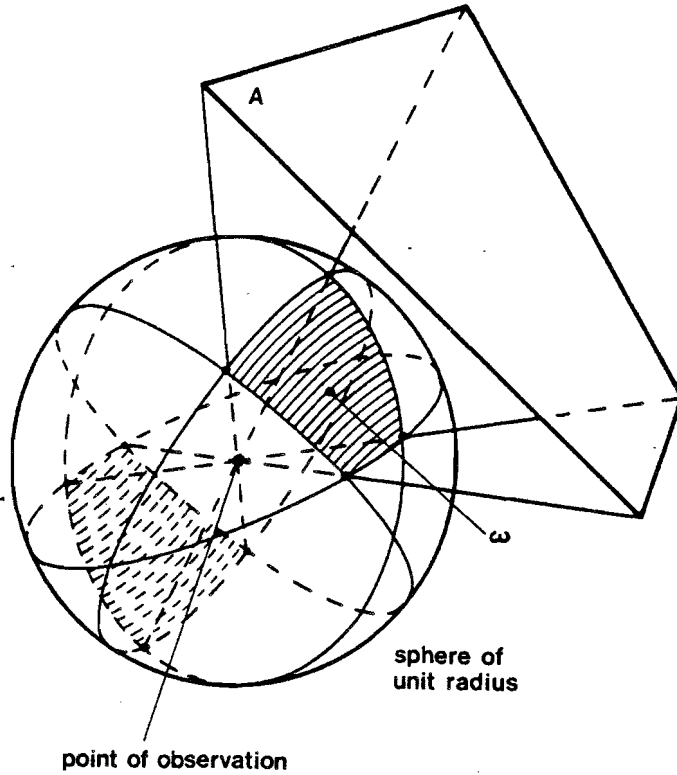
Figure A.3

Todhunter and Leatham (1911) give an expression for the area of the projection of a polygon on a sphere with radius r_a. In our situation, we have a quadrangle and a sphere of radius $r_a=1$, the expression is as follows:

$$\omega = (\alpha_1 + \alpha_2 + \alpha_3 + \alpha_4) - 2\pi \qquad A.8$$

The angles $0 \leq \alpha m \leq \pi$ are illustrated in Figure A.4. They can be found by calculating the unit vectors along the normals of the including planes n_1 and n_2 (Figure A.5).

$$\alpha = \arccos(-\underline{n}_1 \cdot \underline{n}_2)$$
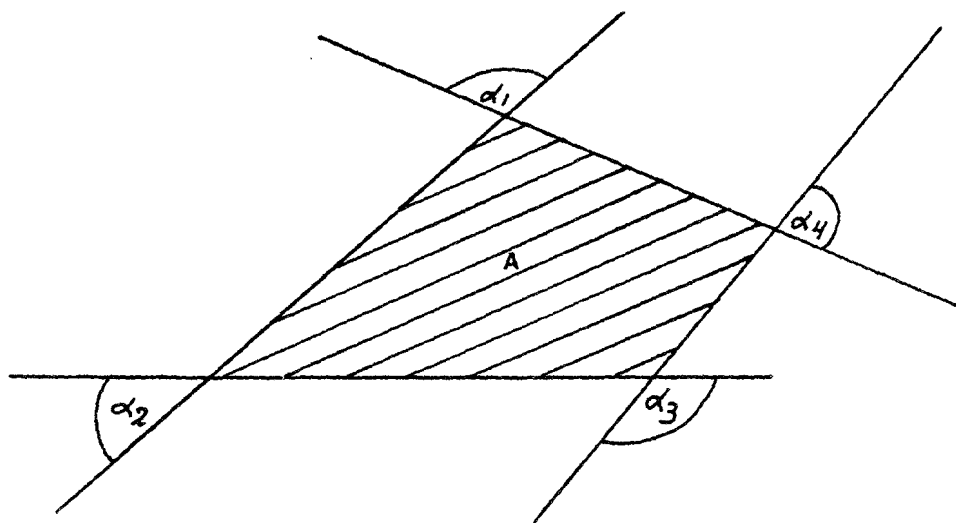
Figure A.4
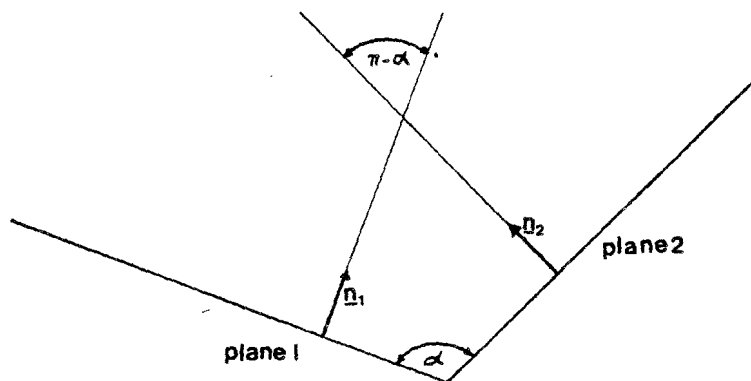
Figure A.5

The contour of a quadrangle consists of four sides. Along such a side, $\underline{\tau} = \underline{\tau}_m$ is a constant vector (see table 2.1). Further we introduce (Figure A.6):

$$\underline{r}' - \underline{r} = \underline{\rho}_m + \lambda \underline{a}_m \quad \text{with} \quad 0 \leq \lambda \leq 1 \qquad A.9$$

$$ds = a_m \, d\lambda \qquad a_m = |\underline{a}_m| \qquad A.10$$
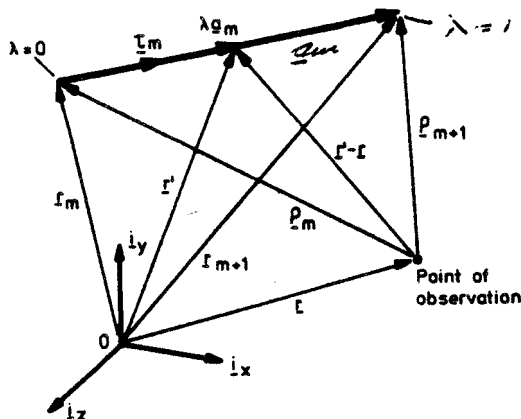
Figure A.6

Now we can write for the contour integral along the m-th side of the quadrangle

$$\int \underline{\tau} R^{-1} ds(\underline{r}') = \int_0^{'} \underline{a}_m R^{-1} d\lambda \qquad A.11$$

in which

$$R = \left[(\underline{a}_m \cdot \underline{a}_m)\lambda^2 + 2(\underline{a}_m \cdot \underline{\rho}_m)\lambda + (\underline{\rho}_m \cdot \underline{\rho}_m) \right]^{1/2} \geq 0 \qquad A.12$$

A.11 now becomes

$$\int_{0}^{1} \underline{a}_m \mathcal{R}^{-1} d\lambda = \underline{a}_m^{-1} L_m \qquad A.13$$

and

$$L_m = \ln\left(\frac{\underline{a}_m \cdot \underline{\rho}_{m+1} + \underline{a}_m \underline{\rho}_m}{\underline{a}_m \cdot \underline{\rho}_m + \underline{a}_m \underline{\rho}_m}\right) \qquad A.14$$

By rewriting A.10 we can see in which cases computing of Lm needs special care. With the help of Figure A.6 we find

$$L_m = \ln\left(\frac{\rho_{m+1}\,(1+\cos(\alpha_m))}{\rho_m\,(1+\cos(\beta_m))}\right) \qquad A.15$$

Two interesting cases arise:

1) $\alpha_m = 0$ and $\beta_m = \pi$
   L_m is singular, so an observation point on a side of the quadrangle is not allowed.

2) $\alpha_m = \pi$ and $\beta_m = \pi$
   The point of observation then lies on the extension of the m-th side along a_m
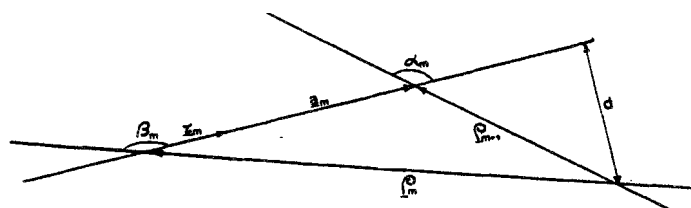
Figure A.7

The distance d can be expressed in terms of ρ_m and ρ_{m+1} and the angles α_m and β_m (Figure A.7)

$$d = \rho_{m+1} \sin(\alpha_m)$$

$$A.16$$

$$d = \rho_m \sin(\beta_m)$$

Considering that α_m and $\beta_m \gg \pi/2$ and using a series expansion we find that

$$\lim_{d \downarrow 0} L_m = \lim_{d \downarrow 0} \ln \left[\frac{\rho_{m+1} \left(1 - \left(1 - \frac{1}{2} \left(\frac{d}{\rho_{m+1}} \right)^2 + \cdots \right) \right)}{\rho_m \left(1 - \left(1 - \frac{1}{2} \left(\frac{d}{\rho_m} \right)^2 + \cdots \right) \right)} \right]$$

$$\ln \left[\frac{\rho_m}{\rho_{m+1}} \right] \qquad A.17$$

So finally we have come to the following equation, the magnetic-field strength of a plane homogeneously charged quadrangle:

$$\underline{H}_A(\underline{r}) = \frac{-\sigma_M}{4\pi} \left\{ \left(\sum_{m=1}^{4} (\underline{n}_\varphi \times \underline{s}_m) L_m \right) + \underline{n}_\varphi \Omega \right\} \qquad 2.13$$

APPENDIX B

DERIVATION OF A CHARACTERISTIC OF TWO-DIMENSIONAL HEAD
CONFIGURATIONS

We define D as a part of two-dimensional space (vacuum
$\mu=\mu o$):

$$\mathcal{D}: \quad -\infty < x < \infty \qquad\qquad y > 0$$
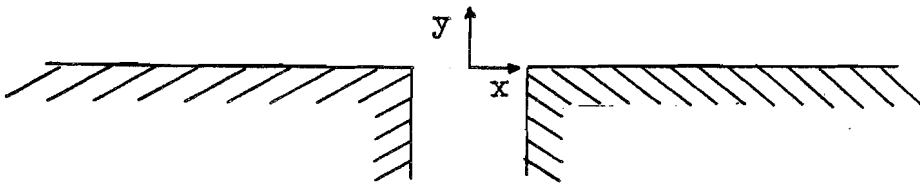
Figure B.1

The equations of Maxwell for two-dimensional magnetostatic
problems without currents in D:

$$\nabla \times \underline{H} = \underline{0}$$

$$\nabla \cdot \underline{H} = 0 \qquad\qquad B.1$$

so:

$$\nabla \times \nabla \times \underline{H} = \underline{0}$$

$$\nabla (\nabla \cdot \underline{H}) = \underline{0} \qquad\qquad B.2$$

Now we can use a vector identity:

$$\nabla (\nabla \cdot \underline{H}) = \nabla^2 \underline{H} + \nabla \times \nabla \times \underline{H} \qquad\qquad B.3$$

$$and \quad \nabla^2 \underline{H} = \underline{0} \qquad\qquad B.4$$

In components:

$$\frac{\partial^2 H_x}{\partial x^2} + \frac{\partial^2 H_y}{\partial y^2} = 0$$

$$\frac{\partial^2 H_y}{\partial x^2} + \frac{\partial^2 H_y}{\partial y^2} = 0$$

$$B.5$$

Taking the Fourier Transform of B.5 with respect to x (1.5b) we obtain:

$$\partial_y^2 \tilde{H}_x - k^2 \tilde{H}_x = 0$$

$$\partial_y^2 \tilde{H}_y - k^2 \tilde{H}_y = 0$$

$$B.6$$

The solution of B.6 is:

$$\tilde{H}_x(k;y) = \tilde{H}_x(k;0) \, e^{-|k|y}$$

$$\tilde{H}_y(k;y) = \tilde{H}_y(k;0) \, e^{-|k|y}$$

$$B.7$$

where we assume that $H_x(k;0)$ and $H_y(k;0)$ are known.

The Fourier Transform of $\underline{\nabla} \cdot \underline{H} = 0$ is:

$$-jk\tilde{H}_x + \frac{\partial}{\partial y} \tilde{H}_y = 0 \qquad B.8$$

because

$$\int_{-\infty}^{\infty} \frac{\partial H_y}{\partial y} e^{jkx} \, dx = \frac{\partial}{\partial y} \int_{-\infty}^{\infty} H_y \, e^{jkx} \, dx = \frac{\partial}{\partial y} \tilde{H}_y \qquad B.9$$

Substitution of B.7 in B.8 brings us to

$$-jk\,\tilde{H}_x(k;o) - k\,\tilde{H}_y(k;o) = 0 \qquad\qquad B.10$$

$$\tilde{H}_x(k;o) = j\,\tilde{H}_y(k;o) \qquad\qquad B.11$$

With B.8 we find:

$$j\,\tilde{H}_x(k;y) = \tilde{H}_x(k;y) \qquad\qquad B.12$$

$$|\tilde{H}_y(k;y)| = |\tilde{H}_x(k;y)| \qquad\qquad B.13$$

So for two-dimensional head configurations the moduli of the sensitivity functions are equal.

In order to make an inverse Fourier Transform possible one should derive an expression for the case ($k < 0$) too. In this case also B.13 is found, the derivation is omitted here.

APPENDIX C

THE MATHEMATICAL FORMULATION OF PADDY

In this appendix we describe how, in our case, a system
of linear equations is achieved. The solution of this system
is not treated.

The equations of Maxwell that describe a magnetostatic
problem with currents and permanent magnets as sources are:

$$\nabla \times \underline{H} = \underline{J} \qquad\qquad C.1$$

$$\nabla \cdot \underline{B} = 0 \qquad\qquad C.2$$

With B_r as the remanent induction (Tesla:T) we have:

$$\underline{B} = \mu \underline{H} + \underline{B}_R \qquad\qquad C.3$$

Firstly we define H   as the field from the currents
when all the magnetizable materials are omitted from the
problem. So

$$\nabla \times \underline{H}_j = \underline{J} \qquad\qquad C.4$$

$$\nabla \cdot \underline{H}_j = 0 \qquad\qquad C.5$$

This field $\underline{H}_j$, also called primary field, can be calculated
explicitly via Biot-Savart's law (Stratton, 1941). If we
restrict space to a part where $\underline{J} = \underline{0}$ and, if necessary, insert
cuts to make it simply connected, we can define a potential
U_j by:

$$\underline{H}_j = -\nabla U_j \quad (\text{where } \underline{J} = \underline{0}) \qquad\qquad C.6$$

* to reduce writing most arguments are omitted

Returning to the original problem, we define

$$\underline{H} = \underline{H}_m + \underline{H}_j \qquad C.7$$

By taking the curl on both sides, we see that $\underline{\nabla} \times \underline{H}m = \underline{0}$ everywhere, so there exists a potential U_m such that:

$$\underline{H}_m = -\nabla U_m \qquad C.8$$

This is called a reduced potential. If space is restricted again, one can define a total (or full) potential $U_f = U_m + U_j$ such that:

$$\underline{H} = -\nabla U_f \quad (\text{where } \underline{J} = \underline{0}) \qquad C.9$$

In materials with high μ, $\underline{H}_m$ is almost equal to $-\underline{H}_j$, giving rise to numerical cancellation problems. Therefore it is advantageous to use the total potential in these areas. So we split space into two parts, one called T_f, containing the region with high μ, the other T_j, containing the region where the current floor. Other regions (e.g. the air) may be included in either of these. We will solve the following equations.

$$\underline{\nabla} \cdot \underline{B} = \underline{\nabla} \cdot (\mu(-\nabla U_m + \underline{H}_j) + \underline{B}_R) = 0 \text{ in } T_j \qquad C.10$$

$$\underline{\nabla} \cdot \underline{B} = \underline{\nabla} \cdot (\mu(-\nabla U_f + \underline{B}_R) = 0 \text{ in } T_f \qquad C.11$$

At the interface between T_j and T_f the potential U_f is discontinous. The jump is equal to U_j. This quantity is calculated in advance using the normal component of H_j as a boundary condition in the equation that follows after substitution of C.6 in C.5:

$$\nabla \cdot (\nabla U_j) = 0 \qquad C.12$$

If no currents are present in the problem we have an expression like C.11 that applied for the whole region $T=T_j+T_f$, bounded by the surface S. Since nothing essential is left out, we will continue with an expression like C.11:

$$\nabla \cdot \underline{B} = \nabla \cdot (-\mu \nabla U + \underline{B}_R) = 0 \qquad C.13$$

For computational reasons T has to be restricted to a finite domain in space bounded by S. Furthermore we will only consider problems with materials for which: μ_r= constant.

A weak solution of C.13 can be found with the distribution (Strang and Fix, 1973)

$$\iiint_T \omega \nabla \cdot \underline{B} \, dT = 0 \qquad \forall \omega \in \overline{K} \qquad C.14$$

$\overline{K}$ is a set of so-called test functions.

We can rewrite C.14 into:

$$-\iiint_T \underline{B} \cdot \nabla \omega \, dV + \iiint_T \nabla \cdot (\omega \underline{B}) \, dV = 0 \qquad C.15$$
$$\forall \omega \in \overline{K}$$

$$-\iiint_T \underline{B} \cdot \nabla \omega \, dV + \oiint \omega (\underline{B} \cdot \underline{n}) \, dS = 0 \qquad C.16$$
$$\forall \omega \in \overline{K}$$

Boundary conditions imposed by the user determine the value of the surface integral in C.16.

From now on we approximate:

- the space $\bar{K}$ by a finite set K (N test functions)
- the solution U($\underline{r}$) by

$$U(\underline{r}) = \sum_{i=1}^{N} U_i(\underline{r}_i)\, \omega_i(\underline{r}) \qquad \omega_i \in K \qquad C.17$$

In C.17 we suppose that it is sufficient to determine the potential in a number of N nodes $\underline{r}_i$ in T. The functions $\omega_i(\underline{r})$ are again chosen out of set K.

Substitution of C.16 and C.17 in C.13 brings us to:

$$\iiint_T \mu \sum_i U_i \, \nabla\omega_i \cdot \nabla\omega_j \, dV - \iiint_T \underline{B}_R \cdot \nabla\omega_j \, dV$$

$$+ \oiint \omega_j \, B_n \, dS = 0 \qquad \forall \omega_j \in K \qquad C.18$$

C.18 can be rewritten into:

$$\sum_i U_i \iiint_T \mu \, \nabla\omega_i \cdot \nabla\omega_j \, dV = \iiint_T \underline{B}_R \cdot \nabla\omega_j \, dV$$

$$- \oiint \omega_j \, B_n \, dS \qquad \forall \omega_j \in K \qquad C.19$$

The right-hand side of C.19 is known.

We now have achieved a set of linear equations:

$$\underline{\underline{M}}\ \underline{u} = \underline{X} \qquad\qquad C.20$$

The square matrix M consists of element

$$M_{ij} = \iiint_{T} u \nabla \omega_i \cdot \nabla \omega_j \, dV \qquad\qquad C.21$$

U represents the unknown $U_1, \ldots, U_N$ and $\underline{X}$ the right-hand sides of C.19 for all the test functions ω_j out of K. It can be shown that $\underline{M}$ is a positive definite matrix.

To specify the test functions we first introduce the notion: "mesh". The mesh arises when all the nodes are connected with each other. The basic element from which this mesh is built, is the hexahedron, which is most easily imagined as a distorted cube (Figure C.1). Furthermore we define a function v , mapping the unit cube on the distorted element:
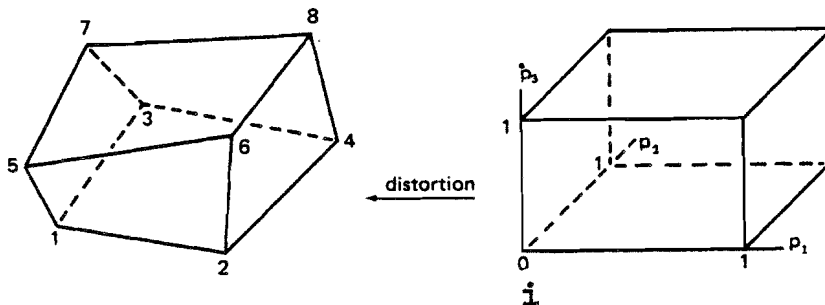

Figure C.1

$$v = f(p_1, p_2, p_3) \qquad\qquad C.22$$

The test function for point i of the element can now be specified:

$$\omega_i(\underline{\vartheta}) = b_i\left(f^{-1}(\underline{\vartheta})\right) \qquad C.23$$

Assuming that f is invertable. The function b for point i in Figure C.1 is:

$$b_i(\mu_1, \mu_2, \mu_3) = (1-\mu_1)(1-\mu_2)(1-\mu_3) \qquad C.24$$

outside the cube bi is zero.

The test functions for the other points of the element can be specified in a similar way. We see in C.17 already that the magnetic potential undergoes the same distortion as the element itself. This is called an iso-parametric way of ap-proximating the solution.

The test functions ω_i are chosen unequal to zero only in the neighbourhood of the nodes. They are called finite elements. Now the contribution of U_i to the potential near node $\underline{r}_i$ is unequal to zero only in the eight mesh elements surrounding $\underline{r}_i$. This results in a sparse matrix $\underline{\underline{M}}$ (C.21), which is solved using the: "Incomplete Choleski Conjugated Gradient" method (I.C.C.G.). We will not treat this method here. An analysis of the finite element method is given by Strang and Fix (1973).

In conclusion we remark, that, since the potential is continuous at the surface of a mesh element, the tangential component of B is continuous. The fact that the normal com-ponent of B is not continuous is called: "the element ef-fect".